STYRELSEN FÖR

VINTERSJÖFARTSFORSKNING

WINTER NAVIGATION RESEARCH BOARD

Research Report No 25

ON CONDITIONS FOR THE RISE OF SELF-EXCITED ICE-INDUCED AUTONOMOUS OSCILLATIONS IN SLENDER MARINE PILE STRUCTURES

BY MAURI MÄÄTTÄNEN

Sjöfartsstyrelsen
Finland

Finnish Board of Navigation

Sjöfartsverket
Sverige

Swedish Administration
of Shipping and Navigation

ON CONDITIONS FOR THE RISE OF SELF-EXCITED ICE-INDUCED AUTONOMOUS OSCILLATIONS IN SLENDER MARINE PILE STRUCTURES

MAURI MÄÄTTÄNEN

Department of Mechanical Engineering

University of Oulu

F O R E W O R D

The Winter Navigation Research Board presents its research report no 25. The report deals with the vibrations in a slender bottom founded pile structure under ice load. This study is carried out as a part of an effort to develop new less expensive respective more relaible constructions to replace conventional concrete cassoon lighthouses and anchored marking buoys in Finnish waters.

The Winter Navigation Research Board expresses its thanks to Mr. Määttänen and his assistants for an excellent work.

Helsinki and Norrköping April 1978

Jan-Erik Jansson Lennart Johansson

ACKNOWLEDGEMENT

This work was carried out in the Institute of Technical Mechanics, University of Oulu, during the years 1976 to 1978. It is continuation of the research project by the Finnish Board of Navigation which started at the end of 1974 after the occurence of vibration problems in steel lighthouses on the Gulf of Bothnia.

I would like to express my gratitude to the staffs of the Department of Mechanical Engineering and the Institute of Data Processing Science for offering me good facilities and an encouraging atmosphere.

Financially this work has been supported by the Foundation of Technology in Finland and by the Finnish Board of Navigation.

Finally it is my pleasure to thank Mr. R. Brown for correcting the English text and Miss P. Pyörälä for her careful typing.

Oulu, April 1978

Mauri Määttänen

CONTENTS

ABSTRACT

The replacement of conventional massive lighthouses with slender steel lighthouses or buoys with piers entails pronounced vibrational problems during ice loading. In the present study the interaction of a moving ice sheet with slender bottom founded pile structures is studied in a continuous crushing mode.

A mathematical model is formulated by connecting the properties of ice to the dynamic equations of motion of structure through an averaged ice crushing strength curve. The resulting group of differential equations is autonomous and hence ice-induced vibrations in the structure will be self-excited by nature.

The conditions under which vibrations - dynamic instability - are aroused are solved rigorously and approximatively for practical purposes. Limit cycles and their frequencies are solved by numerical integration. The overall capability of the created model is verified by comparing the calculated results of three application structures with those measured and observed in-situ. With the presented model it will be possible to design structures which are more secure against dynamic ice loads.

The qualitative effects of the most important parameters in ice and structure interaction are given. Quantitative results are trend-giving and require more accurate measured ice crushing strength curves. Total damping is observed to be the most paramount of the too little known parameters affecting limit cycles. A comparison of the predicted and measured force plots suggests that ice-induced damping during crushing is considerably greater than pure structural damping.

1 INTRODUCTION

The interaction of moving ice and a structure is a dynamic phenomenon. While approaching the structure single ice crystals undergo gradually increasing stress levels up to yielding, or more illustratively, up to crushing. After this smashed ice pieces are pushed away, upwards, downwards and on either side of the structure while the following parts of the ice sheet continue crushing. Since ice crystals are in random orientation crushing will start on grains with most unfavourable directions. Thus the magnitude of the ice force arising will be somewhat random. In praxis the size of a structure under ice pressure is much greater than single ice crystals, which will yield to an integrated, average ice load. During constant thickness ice sheet crushing considerably greater fluctuations in ice force will occur if conditions exist for elastic deformations of structure or ice to interact with the ice crushing.

Although the problem of dynamic ice and structure interaction is well recognized, the number of published papers attempting to explain or predict it by calculations is very limited. On the other hand a great many field and laboratory experiments have been carried out and are still in process to gather more data. All published ice force plots show typically random distributions but very often, too, saw-tooth like time-dependent ice forces repeat themselves continuously. It is just this loading condition that is most critical, since ice forces may repeat themselves with the natural frequency of the structure yielding to resonance. Illustrative examples are steel lighthouses in the Gulf of Bothnia which suffered structural

failures owing to resonant ice-induced vibrations, /30/. In this case design criteria for conventional blunt and massive lighthouses were used, which resulted in reduced ice forces and cheap construction, but without an awareness that sensitivity to ice-induced vibrations increases with increasing flexibility and decreasing internal damping of the structure.

The first measurements of dynamic ice and structure interaction are by Peyton, ref. /40/ 1966. He measured total ice force against a vertical circular pile that was simply supported by an oil drilling platform. The dynamic response of the platform itself could not be eliminated from the measurements. Observations and recordings revealed at low velocities sharp ratcheting force oscillations with a frequency of about one cycle per second. Although the natural frequency of the platform was also one cycle per second, Peyton concluded, relying on additional laboratory tests, that ice properties were primarily governing the crushing frequency. He suggested a characteristic failure frequency of one cycle per second for Cook Inlet ice conditions regardless of the fact that plotter recordings also show ice force frequencies of up to 10 Hz.

Peyton also stressed the importance of ice velocity and temperatures on ice loads. According to laboratory tests with ice samples, crushing strength decreases with increasing loading rate. With high loading rates the ratcheting type of ice failure will not occur and amplitudes of ice force oscillations will be considerably smaller.

In 1970 Gaither /11/ referred to Peyton's tests and said that the oscillatory ice force will have a frequency dependent on ice thickness, temperature and loading rate, but not dependent on the properties of the structure. However, he warns of designs with natural frequencies near one cycle per second.

Blenkarn in 1970 /4/ was the first to suspect Peyton's characteristic ice failure frequency. His conclusions rely on numerous field measurements by strain gauges on in-situ structures and on more comprehensive interpretations of Peyton's tests. Blenkarn measured different crushing frequencies with different structures and different ice velocities and concluded that the ratcheting frequency is governed by ice sheet velocity, structure flexibility and by the dependence of ice sheet crushing strength on loading rate. He states that Peyton's data could also be explained by these parameters.

A very valuable contribution by Blenkarn was to delve into the origin of ice-induced vibrations. He presents the concept of negative damping due to decreasing ice crushing strength with increasing stress rate and suggests that vibrations are self-excited by nature. As an application an example is given of how to calculate the state of instability - conditions under which vibrations arise - for a single degree of freedom structure by comparing the magnitudes of positive internal and negative external dampings.

In 1975 Määttänen /30/ described dynamic ice and structure interaction of relatively flexible steel lighthouses suffering from very severe vibrations. Observed and measured ice crushing frequencies varied from 0.5 to 5 Hz and resonance conditions with both the first and second natural frequencies also occurred. A simple formula was presented to interrelate the crushing frequency with both ice and structure properties. The cause of the vibrations was deduced to be self-excited and two years later another paper /32/ was published in which stability and limit cycles of ice-induced vibrations were studied starting directly from the nonlinear, stress rate dependent ice crushing strength curve.

Neill in 1976 /35/ considered the conclusions of both Peyton and Blenkarn regarding the origin of ice induced vibrations.

He was inclined to support Peyton's characteristic ice failure frequency and gives an explanation for observed large range of frequencies, supposing that as ice tends to break into fragments of a certain size, the size together with velocity determines the crushing frequency.

Matlock & al., 1969 /26/ proposed a mechanical model to simulate the observed ice and structure interaction problem. With this model structural responses were achieved similar to those measured. Although the significance of some structural parameters could be clarified, the actual ice and structure interaction could not be predicted, since no physical ice parameters were included in the model.

Reddy & al. /42/ have treated the ice and structure interaction as a random phenomenon. Their method is valuable in predicting the random response of structures under ice loads. Measured power spectras of ice forces or response are generalized and adopted for use in other actual structures. From the structural safety point of view the random response is not, however, so critical as the response of resonant ice forces. Also the applicability of generalized spectras is rather limited since the effect of ice crushing strength is strongly nonlinear in ice and structure interaction.

The main object of most field and laboratory tests, /3, 5, 6, 10, 16, 18, 19, 31, 34, 36, 46, 47, 55, 56/, with ice crushing against a pile, has been to measure the maximum and average ice loads, the effect of pile diameter on ice thickness ratio and the effect of ice velocity on it. Observations of dynamic behaviour have been more of a by-product. In addition to random ice force fluctuations crushing frequencies ranging from 0.5 to 10 Hz have been recorded. This range usually covers the range of the lowest natural frequencies of structures as well.

The effects of temperature and ice sheet velocity have been measured in laboratory tests. Cold ice behaves in a more brittle manner than ice near melting point. With low ice velocities the crushing behaviour is ductile and it changes to brittle when the loading rate has increased sufficiently. After transition to brittle a reduction in average crushing strength also occurs. It is just this reduction which gives rise to self-excited vibrations. In small scale tests the reduction is not clear, /17, 55, 56/, but the majority of measurements, /4, 7, 14, 15, 18, 19, 28, 40, 43, 46, 47, 58/ support an average reduction of crushing strength in the brittle region.

The present study relies on the existence of a decreasing part in the curve of ice crushing strength versus loading rate. The main object is to formulate a mathematical model for ice and structure interaction by connecting the properties of ice to the structure through the crushing strength curve. The model is used to predict conditions for the rise of self-excited ice-induced vibrations in the continuous mode of crushing and their limit cycles. Results will be compared with in-situ observed ice and structure interaction phenomena.

2 ICE AND STRUCTURE INTERACTION MODEL

2.1 General

In this chapter the basis for a mathematical model for ice and structure interaction in continuous crushing is presented. More stress is put on qualitative than quantitative results in predicting conditions for the rise of self-excited vibrations and developing of limit cycles in full-scale structures.

An essential description of this method has been given in a previously published paper /32/, but a more rigorous approach is now presented and the basis for an ice and structure interaction model is considered in more detail. The basic difference with regard to /32/ is that it does not include the dependence of stress rate on polar angle along the periphery of the pile and the dependence of effective crushing strength on pile diameter to ice thickness ratio.

The range of parameters affecting ice and structure interaction is very wide. Deviations in measured ice parameters are usually great and measurements for parameters by eye alone on the arising of self-excited vibrations are not directly carried out. As a result many simplifying assumptions are made and the effect of some parameters omitted. Such phenomena as vibrations with dynamic amplification due to the impact of the ice edge against a pile, rigid body vibrations of an ice floe together with the structure after empinning or ice force fluctuations due to random ice strength and thickness variations are not considered in this context.

2.2 Physical properties of ice

The size of the projectional area of a structure against which ice is crushing is supposed to be so large when compared to the crystal size of ice that analysis need not be carried out at crystal size scale but an average crushing strength σ_c can be used. Hirayama & al. /18/ have observed that σ_c dependence on grain size appears only with $d/d_{cr} < 25$, and Michel & al. /28/ with $d/d_{cr} < 7$ (d = diameter of pile, d_{cr} = diameter of ice crystals). In praxis the grain size of columnar grained ice is from 1 to 20 mm, Gold /14/, increasing with ice thickness. Hence the average crushing strength from the grain size point of view is justified in actual structures.

The properties of ice vary through the thickness of an ice sheet. The main effect is due to temperature profile and salinity. As the thickness of ice is small when compared to the height of a pile, averaging of properties through the thickness does not have any significant effect on structural response or on ice interaction. The effects of grain size and orientation are also handled in a similar way. Natural ice sheets can be regarded in macro scale as orthotropic plates with isotropy in its plane and orthotropy only in the normal direction. The effect of averaged properties can be observed by repeating calculations using a new combination of these parameters for ice crushing strength.

The frequency of ice induced self-excited vibrations with actual structures is so high that the effect of viscoelastic behaviour of ice can be disregarded. According to Gold /14/ the behaviour of ice is essentially elastic if it is loaded to failure within two seconds.

2.3 Dependence of crushing strength on loading rate

The key parameter in ice and structure interaction is the dependence of crushing strength on stress or strain rate. Many researchers have measured crushing strength curves as a function of stress or strain rate /5, 7, 10, 11, 14, 15, 16, 17, 18, 19, 28, 31, 34, 36, 40, 43, 46, 47, 55, 56, 58/. The first was Peyton, fig 2.1, and his results from uniaxial compression tests of Cook Inlet ice samples indicate a decreasing strength with increasing stress rate. A similar trend was also measured on total ice force both with laboratory and with field test piles, /40/. The reduction in failure stress and ice force was about 50 % from the maximum.

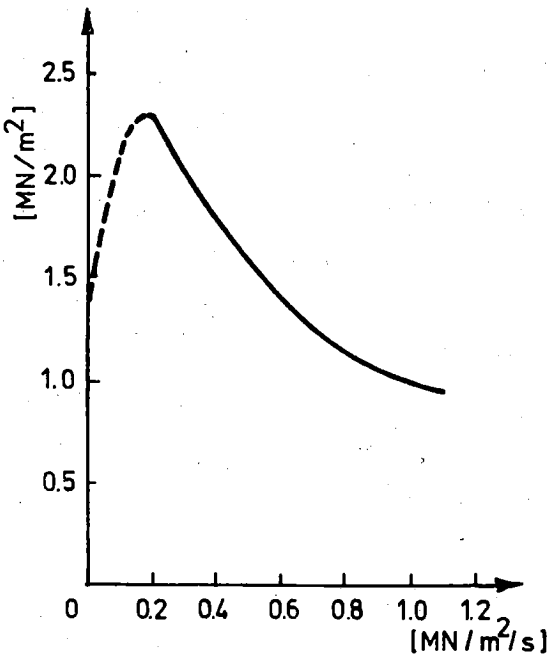

Fig 2.1 Crushing strength vs. strain rate, Peyton /40/

Michel & al. /28/ carried out indentation tests with a square indentor in the laboratory and also collected results from other authors for crushing strength versus strain rate curve, fig 2.2. Ice behaviour is divided into three parts:

a ductile region with a strain rate lower than $5 \cdot 10^{-4} s^{-1}$, where crushing strength obeys power law with exponent 0.32 in relation to strain rate, a brittle region with a strain rate greater than $10^{-2} s^{-1}$, where crushing strength is constant, and a transition zone between the ductile and brittle regions.

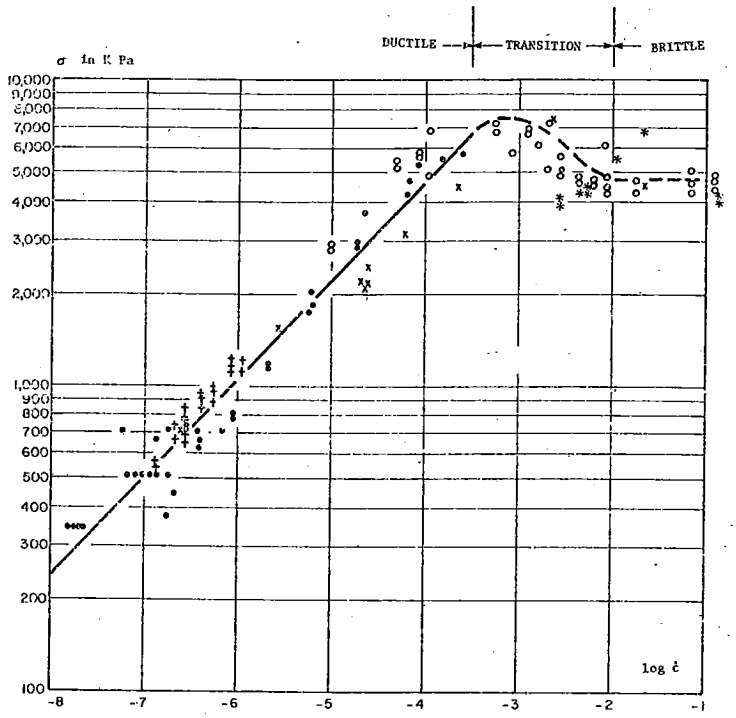

UNIVERSAL CURVE FOR UNIAXIAL CRUSHING AND INDENTATION OF S_2 ICE AT $-10^{\circ}C$,
• — Michel and Paradis (1976) uniaxial
o --- Carter and Michel (1971), uniaxial
† Frederking and Gold (1975), indentation
* Hirayama et Al (1974), indentation,

Figure 2.2 Crushing strength vs. strain rate, Michel & al. /28/

In the brittle region failure occurs more randomly and the above curve represents an average crushing strength. Michel observed thinning of the ice sheet by peeling off wedges from the upper and lower surfaces. Thinning together with strain rate cause an average decrease to about 60 % of maximum at the beginning of the transition zone.

Wu & al. /58/ conducted careful laboratory tests in uniaxial compression and achieved strength-strain rate dependence similar to that of other authors, fig 2.3. In addition they emphasized the effect of temperature: with decreasing temperature the transition from ductile to brittle occurs more abruptly and with lower strain rates. In uniaxial tests the reduction in strength was much greater than in the plane state of stress. The transition to brittle was explained by means of a dislocation theory, according to which with high strain rates dislocation velocity is too low to allow ductile behaviour by plastic yielding and therefore cleavage fracture and linking of grain boundary cracks occur. This also explains well the more random crushing behaviour in the brittle region.

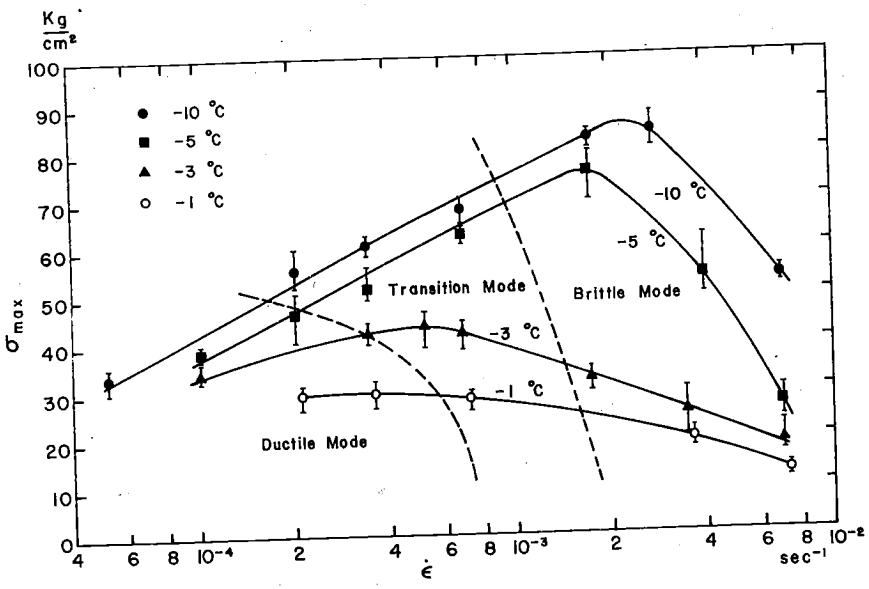

Figure 2.3 Ice crushing strength vs. strain rate and temperature. Wu & al. /58/.

All researchers are of the same opinion with regard to the increasing of ice strength with increasing rate in the ductile region. Almost all agree that maximum occurs in the transition

zone, after which average strength decreases considerably in the brittle region. Nevel & al. /36/ observed in laboratory tests that the speed of an indentor had no effect on crushing strength. However, if stress rates are calculated, see sect. 2.4, it appears that almost all of their data points fall into the brittle region. Haynes & al. /16/ conducted in-situ field tests at Pembina River and got similar results to those of Nevel & al. Again the stress rate is in the brittle region and the report does not mention whether correction due to inertial forces for measured ice forces with high pile velocities was carried out.

Hirayama & al. /18/ measured ice forces with circular indentors and got results that showed the usual reduction in average strength in the brittle region. However, no reduction was observed for a maximum value curve, which was defined in such a way that 90 % of all measured values lie under this curve. Haynes /17/ conducted uniaxial compression tests with dumb-bell-shaped snow ice specimens. His preliminary tests, three samples, indicate that ever-increasing strength values can also be achieved beyond the ductile region. This result is not, however, average but from carefully controlled small test samples, in which probability for initial defects is very low and great strength values can be expected. Comparing this to Hirayama's 90 % curve and Peyton's measurements it can be concluded that for actual structures average reduction in ice strength in brittle region exists. From the structural response point of view, then, it makes no great difference if the reduction is due to strain rate or due to thinning of the ice sheet or uneven contact between ice and structure. The peeling off and local brittle failures occur simultaneously along the contact area, thus yielding to reduction in average ice force.

2.4 Stress and strain rate

Definitions of stress or strain rates according to the theory of elasticity are straightforward. Many variations occur in the definition of strain rate, however. Hirayama & al. /18/ use the concept of fracturing frequency (velocity divided by crushing length per cycle or velocity divided by plastic zone width before indentor). Croasdale & al. /5/ and Michel & al. /28/ take strain rate to be the velocity of an indentor divided by its own width or ice thickness. Physically it is not enough for the definition of strain rate to have the right dimensions only.

Correct strain rate definitions are those of Gold /14/ according to the dislocation theory, and those in uniaxial tests where the velocity of crossheads is divided by the length of the test sample. Starting from the deformation rate Frederking & al. /9/ also correctly define the strain rate.

The strain rate definitions above are valid only for the elastic region. After yielding and during continuous crushing different definitions are required. For instance in a uniaxial test after yielding, when the constant crushing starts, the strain rate will be zero. The physically correct way is to consider a point in the ice sheet approaching the indentor and calculate the time derivative of its deformation history. None of the authors have used this method for strain rate, however.

Blenkarn /4/ and Peyton /40/ both use stress rate as the abscissae for crushing strength. Its definition is simple in uniaxial tests and also in indentor problems. Blenkarn calculates the stress rate by taking the time derivative from the stress history of a point in the ice sheet approaching the identor. Strain rate could then be achieved by dividing the stress rate by the modulus of elasticity, provided that loading to failure occurs in less than two seconds to exclude the effects of viscoelasticity.

In what follows stress rate will be used for two reasons: its physicially sound definition and for the utilization of Peyton's crushing strength curve. Although Peyton's measurements are the oldest they are still the only ones based on sound loading rate definitions in the transition or brittle regions.

2.5 Idealization of $\sigma_c(\dot{\sigma})$

For limit cycle analysis the crushing strength vs. stress rate curve needs to be in an equation form. An accurate enough approximation - maximum error 2.5 % - is achieved by using a fifth degree polynomial for the measured curve, fig. 2.1.

$$\begin{cases} \sigma_c = 0 & \dot{\sigma} \leq 0 \\ \sigma_c = \sum_{n=0}^{5} A_n \dot{\sigma}^n & 0 < \dot{\sigma} < \dot{\sigma}_b \\ \sigma_c = \sigma_b & \dot{\sigma} \geq \dot{\sigma}_b \end{cases} \qquad (2.1)$$

The parameters in eq. 1 depend on chosen values of maximum crushing strength and the relative magnitudes to it at zero stress rate and at high stress rate σ_b. For instance by choosing $\sigma_{cmax} = 2.0\ N/mm^2$, $\sigma_c(0) = 1.33\ N/mm^2$, $\sigma_b = 0{,}67\ N/mm^2$ and $\dot{\sigma}_b = 1.2\ N/mm^2/s$, (index b refers to the beginning point of the brittle region), the parameters A_n have the following values:

$$\begin{cases} A_0 = 1.341\ Nmm^{-2} \\ A_1 = 8.236 \cdot 10^{-2}\ s \\ A_2 = -3.467 \cdot 10^{-1} s^2 mm^2 N^{-1} \\ A_3 = 5.345 \cdot 10^{-1} s^3 mm^4 N^{-2} \\ A_4 = -3.728 \cdot 10^{-1} s^4 mm^6 N^{-3} \\ A_5 = 9.823 \cdot 10^{-2} s^5 mm^8 N^{-4} \end{cases}$$

With linear scaling it is then possible to get different more or less steep crushing strength curves.

While studying the effect of structural or ice parameters on limit cycles a more convenient presentation for crushing strength curve is by four linear pieces, fig. 2.4.

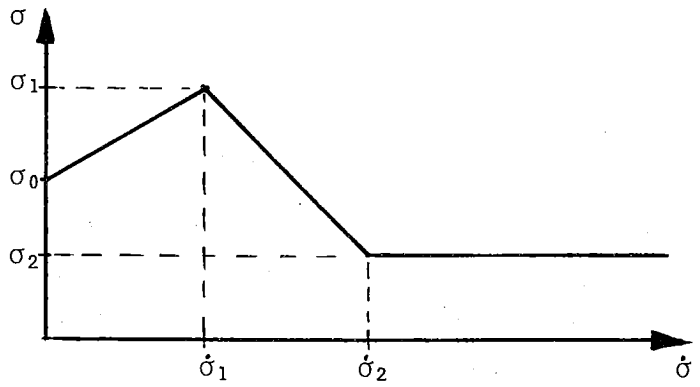

Figure 2.4 Piecewise linear idealization of $\sigma_c(\dot{\sigma})$

Even the effect of parameters directly affecting the rise of self-excited vibrations and limit cycles is most easily found by varying the relations in fig. 2.4. The linearization of the transition zone - the decreasing part of the crushing strength curve - has only an insignificant effect on limit cycles because usually less than 10 % of time in ice and structure interaction occurs in the region $\dot{\sigma}_1 < \dot{\sigma} < \dot{\sigma}_2$ and hence errors in linearization are diminished. In applications the following values were used: $\sigma_0 = 1{,}67$, $\sigma_1 = 2.50$ and $\sigma_2 = 0.83$ N/mm^2, $\dot{\sigma}_1 = 0.20$ N/mm^2/s and $\dot{\sigma}_2 = 0.80$ N/mm^2/s.

2.6 Elastic deformation of ice

Depending on the relative magnitudes of elastic deformation of ice and displacement of structure at the contact area the interaction problem can be divided into three modes: elastic ice displacements are insignificant, displacements of structure are insignificant and both are significant.

In the first mode ice interaction can be taken into account only through the stress rate dependent crushing strength curve. In the second mode the structure is infinitely stiff and its only interaction is reaction force, which for its part is again stress rate dependent. In the third mode both the ice and structure experience elastic displacements simultaneously, and the dynamic equations of equilibrum for both have to be solved simultaneously but separately with the only interconnection by the stress rate dependent ice force at contact points. In each mode the interaction force is calculated following figures 2.1 or 2.4, where the stress rate is a function of the relative velocity v_r between ice and structure

$$v_r = v_0 + \dot{\delta}_i - \dot{\delta}_s \qquad (2.2)$$

where $\dot{\delta}_i$ and $\dot{\delta}_s$ are ice and structure velocities at the contact point and v_0 the initial ice field drifting velocity. Depending on mode, stiffness, damping and mass properties have to be included in the dynamic equations of motion for the structure and/or ice sheet.

In the present study only the case of insignificant elastic ice deformations is considered. This has been done first for the sake of simplicity and secondly because as this is the first research to start from the ice crushing strength curve it is more important to get a qualitative than a quantitative picture of the ice and structure interaction before more accurate ice crushing strength vs. stress rate measurements are available. The characteristics of effects of crushing strength curve on ice and structure interaction appear clearly already in the first mode, where the elastic deformation of ice is supposed to be insignificant when compared with the deflection of the structure at the ice action point. Also observations of the behaviour of an actual structure /30/ suggest that the problem can be simplified in this way, since deflections of up to 200mm in a steel lighthouse under ice loads in

a ratcheting type of crushing were observed while ice in plane deformations was not observed.

The justification of the first mode for slender bottom-founded structures can also be supported by calculations. The elastic displacement u_r of a circular pile in the middle of an ice field is according to Frederking & al. /9/

$$u_r = \varepsilon_r \, a \left[0{,}550\left(\frac{a}{L} - 1\right) + 0{,}450 \ln \frac{a}{L} - 0{,}277\right] \quad (2.3)$$

where ε_r is the maximum radial ice strain at the contact point, $a = d/2$ = radius of pile, and L is the distance to the fixed boundary of the ice field. Evidently infinite ice fields induce infinite displacements in static loading. In praxis all ice fields are finite and the order of magnitude of u_r can be determined by taking a typical pile diameter $d = 1$ m, $\varepsilon_r = 5 \cdot 10^{-4}$ (maximum elastic strain just before yielding in a short duration loading) and varying L/a ratio:

L/a	u_r(mm)
10^2	0.72
10^3	0.98
10^4	1.24
10^5	1.50

Table 2.1 Elastic ice displacement

Displacements of the same order will also result if they are calculated for a semi-circular edge loading in a wide plate according to Girkmann /12/.

The order of L/a ratio in practical calculations can also be bounded by using the wave equation. The elastic stress waves starting from the crushing point proceed with the velocity of sound in the ice. Hence only those boundaries have any effect on ice and structure interaction which lie at a distance smaller than the distance that elastic waves travel in half of the crushing period. As the measured range of

crushing frequencies is from 0.5 to 10 Hz and the velocity of sound in ice is about 2 800 m/s distance L is limited to 2 800...140 m. With a = 0,5 m the maximum L/a ratio is then $5.6 \cdot 10^3$ and the magnitude of u_r is about 1 mm. Eq. 2.3 is not valid on small L/a ratios, but, as can be seen, most of the deformation occurs very far away from the crushing point and if this part of the deformation can contribute to the ice and structure interaction these far away fields should vibrate at the same frequencies as crushing occurs. As this is impossible the magnitude of u_r will be still smaller than in previous calculations.

Without elastic displacement of ice the stress rate is a unique function of the relative velocity between ice and structure. When the stress rate is calculated the crushing strength can be determined either from fig. 2.1 or 2.4.

2.7 Model of structure

In the following only single pile vertical structures are considered. Piers and some lighthouses are typically single-pile bottom-founded slender cantilever structures with large enough displacements to justify the disregarding of elastic deformation of ice. The principles presented are likewise applicable to structures with many legs which may all be under ice loads simultaneously.

As actual structures hardly ever have constant stiffness or mass distributions along their length, a numerical method and the discretization of system was adopted from the very beginning for the self-excited vibration problem. The pile structure is discretized into sufficiently short beam elements with displacement and rotation degrees of freedom at both ends. Conventional finite element methods are then used and a stiffness matrix [k] and consistent mass matrix [m] formed for the elements and the whole structure are assembled. The added mass due to

the surrounding water is observed using the displaced volume concept, Skop & al. /48/.

Element lengths are usually many times the thickness of ice. In this case for simplicity one node can be positioned at the point of ice action so that the ice load can be directly inserted to within only one degree of freedom in the loading vector.

2.8 Damping

Most structural and hydrodynamic dampings are nonlinear in relation both to deformation and its time derivative. The usual concept to linearize damping is to use equivalent linear damping coefficients, Lazan /23/. As damping forces are usually very small when compared with stiffness or mass forces the vibratory response deteriorates only insignificantly while the nonlinear damping dissipates as much energy per cycle as the linear viscous damping.

The problem of self excited vibrations, however, is more pronouncedly damping dependent. For limit cycles or stability in the large the energy dissipation concept - equivalent viscous damping - is accurate enough, but for stability in the small it is necessary to know the shape of the damping curve. Following Tondl /51/ the situation may be visualized in figures 2.5 a and b.

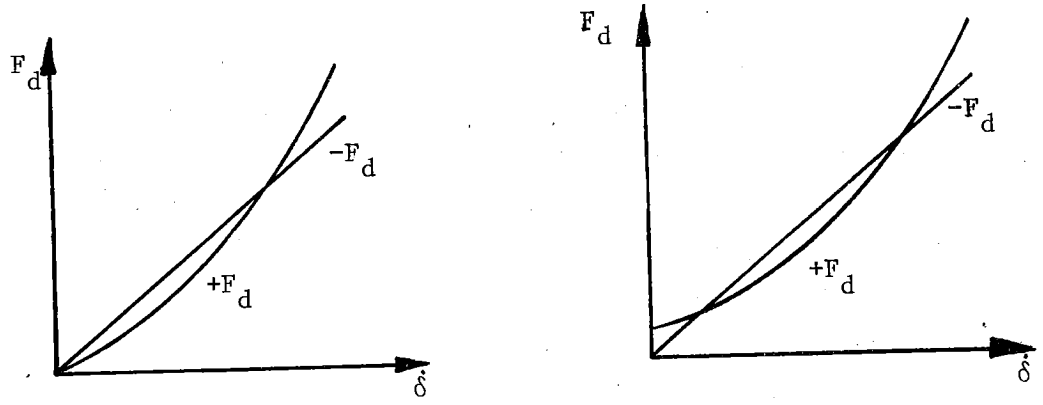

Figure 2.5 Effect of damping curve shape

By considering the negative damping due to ice crushing to be linearily dependent on velocity $\dot{\delta}$, it can be seen that in case a) the rate of negative damping is greater at the start than the rate of positive damping force, making the origin unstable. In case b) the rates of damping forces are equal to those in case a), but now the positive damping includes a constant part, which makes the origin stable. Both cases have stability in the large.

Damping in structures is hysteretic and only slightly or not at all dependent on the rate of loading, Lazan /23/. Together with hydrodynamic damping, which is linear in small Reynolds numbers and nonlinear with higher, structures under ice loads have damping curves more like the type in case b), although the constant part is small.

By regarding the descending part of the ice crushing strength curve as negative damping and by inserting the velocity origin at the steepest point of descent in the crushing strength curve the negative damping effect of ice is schematically according to fig. 2.6.

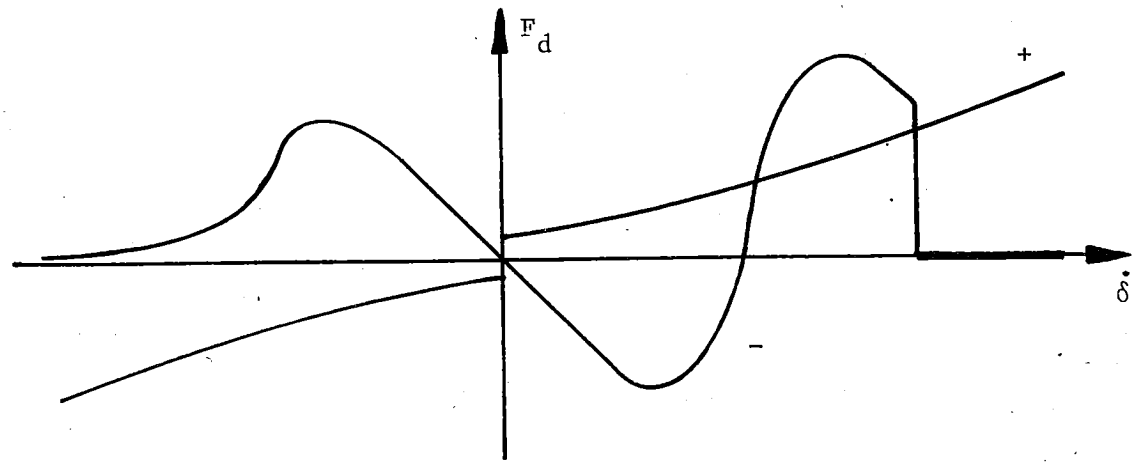

Figure 2.6 Ice force vs. velocity $\dot{\delta}$

When structural and hydrodynamic dampings are presented schematically in the same picture it can be seen that the origin is stable owing to rate independent structural damping, but even a very small change in velocity $\dot{\delta}$ makes the situation unstable. Thus intuitively the origin is always stable in the small. On the other hand it is evident that stability in the large always exists.

If the curve of positive damping is linearized the greatest error will be just near the point of origin, where stable origin may be predicted as unstable. However, because at the point of origin the question is one of stability in the small, this has no practical significance since ever-present randomness, especially in the transition and brittle region, in ice forces will push the point of action to the intermediate instability region, and what is left is again the question of stability in the large.

From the structural safety point of view the linearization of the positive damping curve means operating on the safe side in the problem of ice and structure interaction. Damping details themselves would need a separate study of their own in the case of a bottom founded marine structure and do not come within the scope of this work. Remembering the deviations in ice properties conventional linearized damping of structure is considered accurate enough in this context.

The negative damping effect of ice is observed following the ice crushing strength curve with relative velocity. In addition ice crushing also includes positive damping. These effects are the energy required to crush and grind ice into small pieces, pushing pieces away and friction between ice and structure. Partly these effects are taken into account already in the ice crushing strength curve, where in the brittle region the average ice force value is used instead of considering it to be zero after bursting like failure of ice. In ductile region positive ice damping effects are negligible -

practically no crushing - and therefore no additional positive ice damping effects are included in the damping model of structure.

The structural and hydrodynamic dampings are observed using principal mode relative damping coefficients. These have been reported to be from 2 % by Blenkarn /4/ up to 6 % by Matlock /26/. Ross /45/ reports a value of 2.5 % for a steel tube vibrating freely. Peyton /40/ states that damping is great and Määttänen /30/ also observed great damping, even over-critical, on a steel lighthouse.

Together with ice and water effects it is very difficult to obtain exact damping coefficients. It is premature of Blenkarn to conclude that dampings are small, since in the same paper he also states that decreasing ice crushing strength can be regarded as negative damping. Hence the positive structural and negative ice dampings interfere. As for the structure and water alone without ice effects relative linear damping coefficients of from 3 to 6 % are reasonable for the lowest modes, rising to 10 % with higher modes.

Limit cycles are integrated using principal mode presentation in which modal damping coefficients can be used directly. For stability calculations the damping matrix $[d]$ is required. It is created starting from modal damping coefficients and using the eigenvectormatrix $[X]$ transform, Timoshenko & al. /50/:

$$[d] = [m][X]\lceil M\rfloor^{-1}\lceil D_{ii}\rfloor\lceil M\rfloor^{-1}[X]^{T}[m] \qquad (2.4)$$

where $\lceil D_{ii}\rfloor = \lceil 2\zeta_i\omega_i M_{ii}\rfloor$ is a diagonal matrix of modal dampings with ζ_i = the modal relative damping coefficient, ω_i = natural angular velocity and M_{ii} the principal mode mass in mode i.

2.9 Ice force

A typical expression for ice force acting against a vertical pile is eq. 2.5 by Neill /35/:

$$F = c\kappa\sigma_c hd \tag{2.5}$$

where h is ice thickness, d = pile diameter, σ_c = crushing strength, c = geometrical coefficient = 0.9 for a circular pile, and coefficient κ takes into account the observed dependence of ice force from diameter to ice thickness ratio, fig. 2.7.

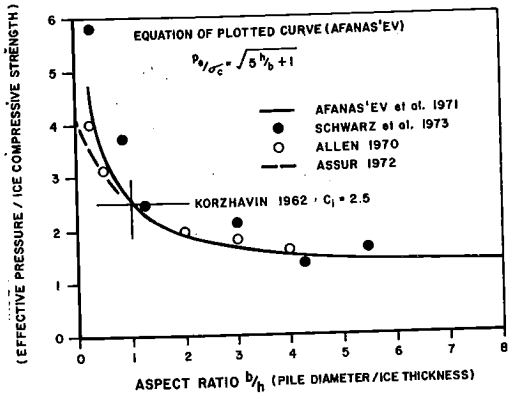

Figure 2.7 The dependence of effective σ_c on d/h, Neill /35/.

The dependence of ice force on diameter to thickness ratio has been studied and measured widely, /1, 2, 5, 10, 16, 19, 28, 35, 36, 46, 55, 56/. Frederking, Gold and Michel are of the opinion that an increase in effective crushing strength with small d/h ratios results from the strain rate effect. Considering a constant strain rate and using the power law in the ductile region a somewhat similar curve to fig. 2.7 is achieved.

In addition to, or included in, coefficients c and κ two other phenomena occur during ice crushing and have an effect on ice force. In the ductile region a small area of ice becomes plastic before the pile, which increases the effective diameter. The plastic region is not very wide but it extends more in the direction of ice movement, about 1.6 · d with flat indentor, Michel & al. /28/. Schematically for a circular pile the situation is according to fig. 2.8. Thus the effective radius, which is required in calculating stress rate, does not increase significantly. The increase in effective diameter further increases ice force with low d/h values, since pushing away crushed ice pieces then requires relatively more tolerance between elastic ice and pile. Maybe this is one of the reasons for the diameter to ice thickness effect. In any event, the increase of diameter is most naturally observed in the aspect ratio coefficient κ and in applications it is further supposed that the measured κ values include this effect.

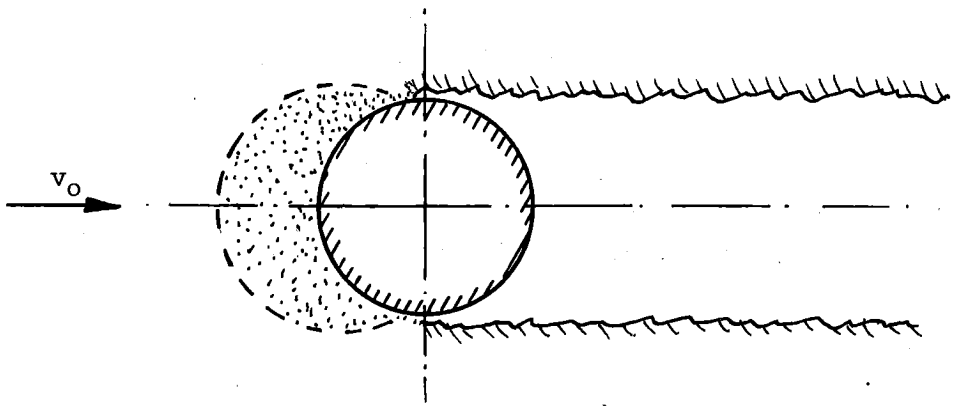

Figure 2.8 Plastic zone in crushing

In the brittle region the crushing phenomena include thinning of the ice sheet by peeling off wedges from the upper and lower surface, Michel /28/. This yields a decrease in the ice thickness in eq. 2.5, which is again treated in such a way that it is supposed that average measured ice crushing strength curves include this effect.

Denoting by v_0 the velocity of the ice field and by $\dot{\delta}_i$ the velocity of the pile at the point of ice action the stress rate is calculated according to Blenkarn /4/ from the equation

$$\dot{\sigma} = (v_0 - \dot{\delta}_i)\frac{4\sigma}{\pi a}c \qquad (2.6)$$

But as σ_c is a function of $\dot{\sigma}$ and as it was measured in uniaxial compression it is also a function of polar angle θ, fig. 2.9.

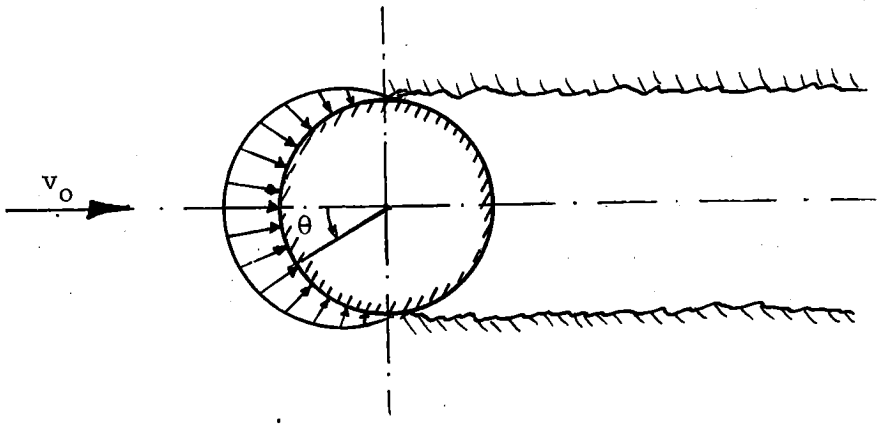

Figure 2.9 Ice pressure against a pile

The radial pressure of rigid circular pile follows approximately the cosine law, Frederking & al. /9/. Thus a more complete equation for ice stress rate will be yielded

$$\sigma_c(\dot{\sigma}, \theta) = \sigma_c(\dot{\sigma}) \cos \theta \qquad (2.7)$$

$$\dot{\sigma} = (v_0 - \dot{\delta}_i) \cos^2 \theta \frac{4\sigma_c(\dot{\sigma})}{\pi a} \qquad (2.8)$$

Using the piecewise linear approximation for the crushing strength curve, fig. 2.4,

$$\sigma_{cj} = \alpha_j + \beta_j \dot{\sigma} \qquad (2.9)$$

stress rate for each region j can be calculated in closed form

$$\dot{\sigma}(\theta) = \frac{\alpha_j}{\frac{\pi a}{4(v_0 - \dot{\delta}_i)} \cos^2\theta - \beta_j} \tag{2.10}$$

It can be proved that the denominator never becomes zero or negative. In the case of figure 2.1 and polynomial expression of σ_c the stress rate have to be solved by iteration, or by expressing $\dot{\sigma}$ as the function of $\dot{\delta}_i$ directly. The latter may be accomplished in such a way that by iteration $\dot{\sigma}$ is solved in so many different $\dot{\delta}_i$ values that a fifth degree polynomial can be expanded in $\dot{\delta}_i$. The ice force F is then integrated:

$$F = h \cdot 2 \int_0^{\frac{\pi}{2}} \sigma_c(\dot{\sigma},\theta) \cos\theta \, a d\theta \tag{2.11}$$

While using fig. 2.4 approximation, depending on stress rate, the integration has to be divided into one, two or three pieces, in which integration boundaries are calculated from eq. 2.10. In the computer program the integration itself is carried out numerically using three point Gauss-Legendere quadrature, which integrates exactly polynomials up to the fifth order. Although σ_c approximations are linear or fifth order the integration will be approximate owing to cosine terms.

2.10 Dynamic equations of equilibrium

Denoting by $\{\delta\}$ the vector of displacements for the discretisized structure, the dynamic equations of equilibrium for the first mode ice and structure interaction problem can be written by compiling the previous sections:

$$[k]\{\delta\} + [d]\{\dot{\delta}\} + [m]\{\ddot{\delta}\} = \{F(\{\dot{\delta}\})\} \tag{2.12}$$

The dot above δ represents its time derivative and thus $\{\dot{\delta}\}$ is velocity and $\{\ddot{\delta}\}$ acceleration vector. The force vector $\{F\}$ is nonzero everywhere but in those degrees of freedom which have contact with ice. In a single pile structure only one term is nonzero and it is calculated from eq. 2.11.

3 DYNAMIC STABILITY

3.1 General

The dynamic equations of equilibrium, 2.12, do not contain time as an independent variable and hence the system is autonomous. As the velocity and properties of ice are kept constant vibrations will occur only if the state of equilibrum is dynamically unstable.

In the case of ice-induced self-excited vibrations the concept of stability can be divided into two groups: orbital stability in the origin and stable limit cycles. In the first case no vibrations at all will arise and in the second case the vibrations will occur but amplitudes will grow only finitely and after a while reach a steady level, limit cycles. In the latter case the exact definition is asymptotically orbitally stable. Moreover the origin can be regarded as a stable limit cycle with zero amplitude.

The definions of Andronov & al. /2/ describe well the behaviour of the whole system: stability in the small and stability in the large. Stability in the small means a restriction for amplitudes within which the origin is asymptotically stable. This situation may be the result of rate independent damping characteristics as stated in sect. 2.8, or of linearized damping when the dynamic equations of motion are not formed in the descending part and especially in the steepest descent point of the ice crushing strength curve. A great enough amplitude may then move the point of action to the unstable region and the question of stability in the large will arise.

In vibration text books and published papers many methods have been presented for determining the nature of the state of equilibrum, /2, 20, 21, 24, 25, 27, 38, 51, 52, 53, 54/. In nonlinear problems the usual approach is to linearize the original problem in the close vicinity of the point in question and then deduce the nature of the state of equilibrium. This approach is also appropriate for ice induced vibrations since the stability only calculations should be carried out at the steepest point of descent in the crushing strength curve, where locally only small nonlinearities appear, see figures 2.1 and 2.2.

The methods for finding out stability in general, method of damping determinant, Routh-Hourwitz method, methods of Liapunov, and others that do not give information about which natural mode stability or instability appears are not sufficient for design purposes. In the case of ice-induced vibrations instability may exist in such a high mode that it has no practical significance. In this chapter only those methods are considered that are capable of giving information about which natural modes stability or instability occurs in. The methods presented are the exact root extraction method, numerical integration method and a simple approximative method.

As the dynamic equations of equilibrium are linearized and the frequencies and amplitudes for autonomous vibrations are then calculated, it should be emphasized that they are valid only in the close vicinity of the linearization point. The ice crushing strength curve is strongly nonlinear and it appears that nonlinearity will have a great effect on both amplitudes and frequencies. A refinement could be achieved by using perturbation techniques, but a more direct method is to use numerical integration, see chapter 4, which gives both limit cycles - stability in the large - and conditions for stability in the small.

3.2 Roots of the dynamical equations of equilibrium

The nature of an equilibrium state can be deduced from the real parts of the roots of the dynamical equations of equilibrium. Each root is attached to its natural mode and thus the stability of modes is found. If the real part of the root is negative, the mode in question is stable, while the positive real part means instability, and a purely imaginary root a neutral state of equilibrium.

The root extraction was first tried using Aitken iteration and Rutishauser method, but both of them failed in the matrices of eq. 2.12. The root extraction succeeded with QR-algorithm, /57/, using "IMSL"-subroutines, /22/. In this program package the roots of the real matrix are solved using QR-algorithm and Hessenberg transformation. The accuracy of calculated roots - eigenvalues - and eigenvectors is monitored by a condition number, which is relative to error vector length. If the condition number is small, then the accuracy of results is of same order as that of the floating point presentation.

For root extraction - stability only - calculation eq. 2.12 has to be first linearized and then transformed to a group of first order differential equations. The ice force can be divided into two parts: the static component $\{F_0\}$ due to ice crushing strength with the initial constant ice velocity and to the change of relative velocity dependent component $\{F_1\}$

$$\{F(\{\dot{\delta}\})\} = \{F_0\} + \{F_1\} = \{F_0\} + [\phi]\{\dot{\delta}\} \qquad (3.1)$$

The rate dependent force vector can be expressed as a matrix product, in which the coefficient matrix $[\phi]$ is diagonal with nonzero terms φ_{nn} only in ice action point degrees of freedom n. The value φ_{nn} is calculated from the integral 2.11 using chain differentiation

$$\frac{dF}{d\dot{\delta}} = \frac{dF}{d\dot{\sigma}} \cdot \frac{\partial\dot{\sigma}}{\partial\dot{\delta}} \tag{3.2}$$

the application of which gives at the point $\dot{\delta} = 0$

$$\varphi_{nn} = -8\pi h d^2 \int_0^{\frac{\pi}{2}} \frac{\alpha_j \beta_j \cos^4\theta}{\left(\pi d - 8\beta_j v_0 \cos^2\theta\right)^2} d\theta \tag{3.3}$$

The term φ_{nn} can also be interpreted as a negative damping coefficient. By comparing with eq. 2.6 it can be seen that it is independent of diameter d. Hence the negative damping, the cause of ice induced vibrations, depends only on ice thickness and the shape of crushing strength curve.

Observing eq. 3.1 the dynamic equations of equilibrium can be expressed in the form

$$[k]\{\delta\} + ([d] - [\phi])\{\dot{\delta}\} + [m]\{\ddot{\delta}\} = \{F_0\} \tag{3.4}$$

This is transformed to a group of first order differential equations by choosing new variables $\{x\}$

$$\{x\} = \begin{Bmatrix} \delta \\ \dot{\delta} \end{Bmatrix} \tag{3.5}$$

$$\begin{bmatrix} [k] & [0] \\ [0] & -[m] \end{bmatrix} \{x\} + \begin{bmatrix} ([d] - [\phi]) & [m] \\ [m] & [0] \end{bmatrix} \{\dot{x}\} = \begin{Bmatrix} \{F_0\} \\ \{0\} \end{Bmatrix} \tag{3.6}$$

By partitioning eq. 3.6 it can be seen that the first group of equations is directly eq. 3.4 and the lower part an identity. The constant loading vector has no effect on the nature of the state of dynamic stability - it could be eliminated by making origo shift v_0 to the state of static equilibrium - and hence the nature of the state of equilibrium is uniquely defined by the homogenous equation.

$$[A]\{x\} + [B]\{\dot{x}\} = \{0\} \tag{3.7}$$

where $[A]$ and $[B]$ are the coefficient matrices in eq. 3.6. By substituting the trial solution $\{x\} = \{x_0\}e^{\lambda t}$ the conventional eigenvalue problem is achieved

$$[A]\{x_0\} = -\lambda[B]\{x_0\}e^{\lambda t} \tag{3.8}$$

A solution for roots λ and eigenvectors $\{x_0\}$ was tried directly in this form with IMSL-subroutines, but it yielded poor condition numbers. Low condition numbers were achieved by first inverting $[A]$ and using other IMSL-subroutines for the form

$$[A]^{-1}[B]\{x_0\} = -\frac{1}{\lambda}\{x_0\} \tag{3.9}$$

It should be noted that the inversion of $[A]$ requires only the inversion of the positive definite stiffness matrix $[k]$. The matrix product in partitioned form will be

$$[A]^{-1}[B] = \left[\begin{array}{c|c} [k]^{-1}\cdot([d]-[\phi]) & [k]^{-1}[M] \\ \hline -[I] & [0] \end{array}\right] \tag{3.10}$$

The roots λ_j for mode j are usually complex conjugate pairs

$$\lambda_j = \rho_j \pm i\,\omega_j \tag{3.11}$$

The real part ρ_j expresses the net damping in the mode j.
If all roots have negative real parts then the point in question - the point of linearization in the crushing strength curve - is absolutely asymptotically orbitally stable, Urabe /54/.
If the real part of mode j is negative disturbance from the state of equilibrium will exponentially decay and the mode is asymptotically stable. A positive real part means exponentially increasing amplitudes and thus instability.

The imaginary part ω_j expresses the natural angular velocity with which self-excited vibrations will occur in small amplitudes. If damping in mode j, positive or negative, is overcritical the root λ_j will be real and amplitude response aperiodically decreasing or increasing. With cantilever slender bottom-founded lighthouses or piers real only roots appear frequently.

3.3 Numerical integration

The nature of the state of equilibrium can also be deduced by numerical integration. A small disturbance is given for the dynamic equations of equilibrium, eq. 2.12, and then the response integrated numerically, see sect. 4.2. If amplitudes decay after disturbance the state of equilibrium is stable, while on the other hand when amplitude starts to rise the state of equilibrium is unstable.

The numerical integration is noneconomical from the point of view of computer time and it does not tell in which mode instability exists. On the other hand it makes it possible to find out whether the origin is stable only in the small by increasing the initial disturbance. In addition if instability exists the limit cycles are obtained instantly by continuing the integration until constant amplitudes are achieved.

3.4 Method of Tondl

An approximative stability requirement can be calculated simply following the method of Tondl, /53/. Basically it is a perturbation method in which only the first approximation is considered.

The presentation of the Tondl method for a two degree of freedom system is given in ref. /53/. Expansion for a multi-degree of freedom system is derived as follows. First equations 3.1 are quasinormalized using eigenvectors [X], which are solved from the free vibration problem

$$([k] - \omega^2 [m] \{\delta\} = \{0\} \tag{3.12}$$

Multiplying eq. 3.4 from the left by $[X]^T$ and choosing new coordinates, the principal coordinates $\{\delta\}$

$$\{\delta\} = [X]\{\pi\} \tag{3.13}$$

follow the form

$$\lceil K \rfloor \{\pi\} + \lceil D \rfloor \{\dot{\pi}\} + \lceil M \rfloor \{\ddot{\pi}\} = [X]^T \{F_0\} + [X]^T [\phi][X]\{\dot{\pi}\} \tag{3.14}$$

where $\lceil\ \rfloor$ denotes a diagonal matrix. Also the damping matrix will be diagonalized, compare sect. 2.8. The principal modes are connected to each other only through the rate dependent ice force matrix $[\phi]$. (The same would also be true if the ice force had not been linearized). In component form eq. 3.14 is

$$K_{ii}\pi_i + D_{ii}\dot{\pi}_i + M_{ii}\ddot{\pi}_i - \sum_j X_{ji}F_j - \varphi_{nn} \sum_j X_{nj}\dot{\pi}_j = 0 = P_i \tag{3.15}$$

in which all terms are moved to the left side. This form can be regarded as a force unbalance P_i in the mode i. By considering a variation $\delta\pi_i = \xi_i$ to the state of equilibrium, $\{\pi\}$, $\{\dot{\pi}\} = \{0\}$, $\{\ddot{\pi}\} = \{0\}$, the resulting variation in force unbalance will be then δP_i, which will also be zero at the equilibrium point. Expanding δP_i follows

$$\delta P_i = \frac{\partial P_i}{\partial \pi_i}\xi_i + \frac{\partial P_i}{\partial \dot{\pi}_i}\dot{\xi}_i + \frac{\partial P_i}{\partial \ddot{\pi}_i}\ddot{\xi}_i = 0 \qquad (3.16)$$

By performing the derivations and observing that $\frac{\partial \dot{\pi}_j}{\partial \dot{\pi}_i} = 0$, and by denoting H_{ii} the coefficient of the time derivative of variation ξ_i

$$H_{ii} = D_{ii} - \varphi_{nn} X_{ni}^2 \qquad (3.17)$$

a homogenous autonomous differential equation for the first order variation ξ_i is obtained

$$K_{ii}\xi_i + H_{ii}\dot{\xi}_i + M_{ii}\ddot{\xi}_i = 0 \qquad (3.18)$$

which will describe the behaviour of the original differential equation 3.15 in the close vicinity of the equilibrium point. It should be noted that the same result, eq. 3.18, would have been achieved if the variation had been carried out on the nonlinearized ice force.

The stability of mode i is deduced from its roots. By substituting $\xi = Ce^{\lambda t}$ the characteristic equation is obtained and roots for the mode i solved

$$\lambda_i = \frac{-H_{ii} \pm \sqrt{H_{ii}^2 - 4K_{ii}M_{ii}}}{2M_{ii}} \qquad (3.19)$$

Defining angular velocity Ω_i according to the equation

$$\Omega_i^2 = \frac{K_{ii}}{M_{ii}} - \frac{H_{ii}}{4M_{ii}} \qquad (3.20)$$

it is observed that Ω_i approaches the natural frequency ω_i of mode i as net damping H_{ii} approaches zero.

In the case $\Omega^2 > 0$ the stability of the mode i is controlled by the sign of H_{ii} : if $H_{ii} > 0$ the mode is stable and if $H_{ii} < 0$ the mode is unstable. Thus the condition for stability in the small is

$$D_{ii} > \varphi_{nn} X_{ni}^2 \tag{3.21}$$

Expressing D_{ii} using relative modal damping coefficients ζ_i, the stability requirement for internal positive damping is

$$\zeta_i > \frac{\varphi_{nn} X_{ni}^2}{2M_{ii}\omega_i} \tag{3.22}$$

The stability requirement presented in ref. /32/, eq. 2, is in other respects similar to eq. 3.22 but there the term φ_{nn} was calculated following Blenkarn /4/ and regarding the dependence $\sigma_c = \sigma_c(\dot{\sigma}, \theta)$ as constant. Because both the stress rate and σ_c change with θ the effect of negative slope of crushing strength curve is not so severe through eq. 3.3. Thus eq. 3.22 is more rigorous but eq. 2 in ref. /32/ is on the safer side for practical calculations.

The formulation in the above is approximative in two senses. First the original nonlinear ice force becomes linearized and secondly only the first order approximation is used. For the stability only calculations the linearization has no significant effect on accuracy, since in the vicinity of the steepest point of descent in the crushing strength curve nonlinearities are small.

The accuracy of first order approximation is the greater the smaller the terms on the right hand side of eq. 3.15 connecting principal modes. As the only cross-exitation of modes is through φ_{nn} term it is enough to require φ_{nn} to be small in comparison to other forces in the equation of equilibrium.

Unfortunately this is not usually the case in actual structures. In many cases φ_{nn} is so great that aperiodic divergencies in the small will result. This means that quantitatively the first order approximation is not accurate. Qualitatively, however, eq. 3.22 can be used to find out stability regions. The instability boundary lies at the point where $H_{ii} = 0$. Thus $D_{ii} = \varphi_{nn} X_{ni}^2$ and this means that at the instability point the effect of φ_{nn} is of same order as that of internal damping which is small. Hence eq. 3.22 is valid for stable regions and gives qualitatively answers if the mode in question is unstable.

The main advantage of eq. 3.22 is that it gives answers to the question of dynamic stability in simple engineering practice terms which are readily available in dynamic structural analysis algorithms, and that the stability of modes is resolved. An important observation for design purposes is the effect of X_{ni}, the amplitude of mode i at the ice action degree of freedom n. For stable design the structure should be stiff and light - small X_{ni} and high ω_i.

4 LIMIT CYCLES

4.1 Existence of limit cycles

The existence of limit cycles - stability in the large - can be easily postulated by considering the energy balance. The external energy imparted to the structure during ice crushing is proportional to the first power of amplitude at the beginning and remains constant when maximum amplitude has moved the point of action out of the descending part of the crushing strength curve. Internal energy dissipation increases monotonically with increasing amplitudes, and is relative to the second power of amplitude in the case of viscous damping. Sooner or later, then, asymptotically a constant situation develops in which the net energy change is zero during one cycle of vibration and limit cycles are established.

Methods for calculating limit cycles are mostly based on successive approximations or on constructing phase plane plots. Owing to strong nonlinearities in the large and the great number of required degrees of freedom they are not feasible for the ice crushing problem. Numerical integration schemes do not have any difficulties in following the ice crushing strength curve and usually they are readily available in dynamic structural analysis program libraries. Therefore only numerical integration for limit cycles is considered in this context.

4.2 Numerical integration

The dynamic equations of equilibrium 2.12 can be solved using the fourth order Runge-Kutta scheme. To save computer time a principal mode presentation is adopted. After the transformation the left hand side for mode i is the same as that of eq. 3.14 but the right hand side is observed rigorously

$$K_{ii}\pi_i + D_{ii}\dot{\pi}_i + M_{ii}\ddot{\pi}_i = X_{ni}F_n(\dot{\delta}_n) \qquad (4.1)$$

The index n denotes the degree of freedom of the ice action point. If ice action appears at several points the contribution of each must be summed. In each Runge-Kutta step a new ice force F_n has to be calculated. This requires first that $\dot{\delta}_n$ is solved from

$$\dot{\delta}_n = \sum_j X_{nj}\dot{\pi}_j \qquad (4.2)$$

and then the new F_n can be integrated from eq. 2.11 using the three point Gauss-Legendere quadrature.

The Runge-Kutta method is a self-starting scheme. Thus integration can be started with initial conditions $\{\delta\} = \{0\}$ and $\{\dot{\delta}\} = \{0\}$, which describes physically the collision of the ice sheet edge against the pile. The response then includes first the transient to the state of average ice load together with developing limit cycles before steady state limit cycles are established.

From the point of view of pure limit cycles it is better to avoid transition and start integration with initial conditions $\{\delta\} = \{\delta_0\}$ and $\{\dot{\delta}\} = \{0\}$, where $\{\delta_0\}$ is the static displacement vector at the point $v_r = v_0$. Although the integration now starts form the state of equilibrium it has been observed that

numerical errors in double precision eigenvectors usually cause enough disturbance to start self-excited vibrations if instability in the small exists. When required, it is always possible to cause greater disturbances in order to inspect stability in the small, intermittent instability and stability in the large or limit cycles.

As nonlinearities appear only in the loading term it is also easy to take into account the possibility of losing contact with ice and structure. This happens as soon as relative velocity is negative

$$v_r = v_0 - \dot{\delta} \leq 0 \tag{4.3}$$

and thereafter the ice force is zero until the gap is closed again. The condition for new contact according to the symbols in fig. 4.1 is

$$g = \delta_n(t) - \delta_n(t_g) - v_0(t - t_g) \leq 0 \tag{4.4}$$

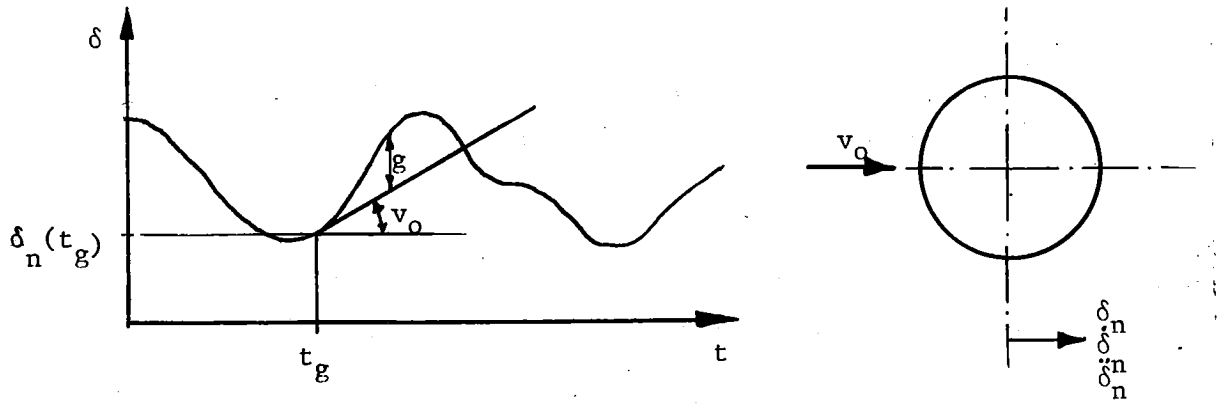

Figure 4.1 Gap between ice and structure

The convergence of the Runge-Kutta method is proved by Urabe in ref. /54/. For convergence it is required that eq. 4.1 is continuous and that Lipschitz condition is satisfied. These requirements are satisfied everywhere else but at the point $\dot{\delta} = v_0$, the point of contact/no contact. This point can be excluded by considering separate solutions for the cases $v_r > 0$ and $v_r < 0$, and using the results from the previous case as initial values for the new case if the point $v_r = 0$ is passed. In nature the ice force curve is not discontinuous, which will be the result when idealized curves are used, fig. 2.2 or 2.4, compare the presentation of Michel /28/ and consider the effect of elastic deformation of ice. Thus discontinuity could also be avoided by different idealization. In practical calculations the time step in Runge-Kutta integration is finite and the change of σ_c at the point $v_r = 0$ can be interpreted as occuring continuously and linearily during one time step. Hence in any case the Lipschitz condition is met.

The principal mode presentation in numerical integration makes it possible to take into account only those modes that have a significant effect on ice and structure interaction. As the interaction is governed by the relative velocity between ice and structure and by the possible gap, it is enough to take into account only those lowest modes that are capable of describing displacement and velocity histories reasonably accurately.

In practical calculations the integration time step is defined according to the highest mode included. The requirement is to have at least 20 time steps for this shortest period. In test runs it was observed that still shorter time steps no longer improved accuracy but about ten times longer time steps start to worsen results and still longer time steps will yield numerical instabilities. The number of modes to be included

was checked in test runs in such a way that more higher modes were included until no significant changes occurred any more in velocity response. It appeared that the 4 to 6 lowest modes are enough for pile structures. With these conditions the integrated response is numerically more accurate than is the accuracy of available ice crushing strength curves.

5 APPLICATION EXAMPLES

5.1 Analyzed structures

For the application of the theory presented in the preceding chapters three different structures have been chosen: a) the Kemi-I steel lighthouse, b) a pier and c) the Kokkola test lighthouse, fig. 5.1. All are slender cantilever type, bottom founded steel piles. The pier is a typical example of those in the Gulf of Bothnia, not an actual pier, and others have also been used in actual ice conditions. Some measurements and many observations are available on their behaviour during ice loading, /30/.

Fig. 5.1 also shows the discretization in the numerical model of structures. The total number of degrees of freedom is twice the number of nodes. The most interesting structural design parameters and calculated natural frequencies are given in table 5.1. Stiffness and mass distributions of analyzed structures vary considerably: lateral stiffness for ice force of the pier is twice the stiffness of the Kemi-I steel lighthouse, and the Kokkola test lighthouse is more than twice as stiff as the pier. The mass of superstructures of the pier is only 5 % of that of Kemi-I and the mass of superstructures of Kokkola test lighthouse is about half that of Kemi-I.

The elastic deformation of ice with all application examples is about 1 mm or less. As the deflection of structures in the design ice load is more than 50 times greater, the requirement presented in sect. 2.6 is well satisfied.

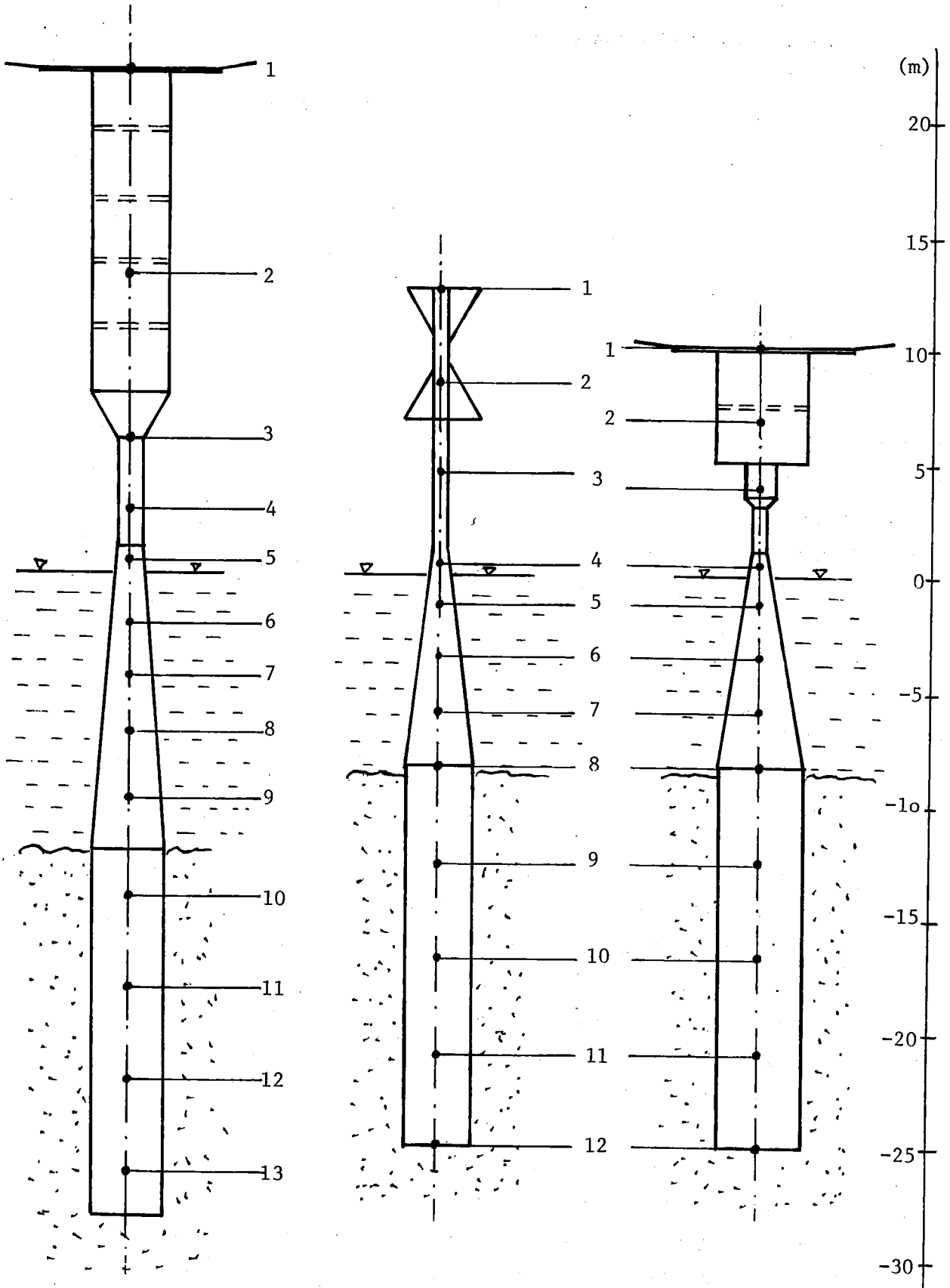

a) Kemi-I steel lighthouse

b) A pier

c) Kokkola test lighthouse

Figure 5.1 Analyzed structures

Table 5.1 Data of analyzed structures

		Kemi-I steel lighthouse	Pier	Kokkola test lighthouse
Top height	m	22.3	12.4	10.0
Water depth	m	12.0	8.7	8.7
Diameter at waterline	m	1.12	0.74	1.06
Design ice thickness	m	1.10	1.00	1.00
Design ice strength	N/mm^2	2.50	2.00	2.50
Design ice force	MN	3.0	4.1	5.2
Lateral stiffness	MN/m	204	441	901
Nominal deflection	mm	147	93	58
Natural frequency f_1	Hz	0.843	2.93	0.432
Natural frequency f_2	Hz	3.81	4.02	1.38
Natural frequency f_3	Hz	8.50	10.6	4.83
Natural frequency f_4	Hz	12.6	14.6	12.4
Modal damping ζ_1	-	0.03	0.03	0.07
Modal damping ζ_2	-	0.05	0.05	0.07
Modal damping ζ_3	-	0.05	0.05	0.09
Modal damping ζ_4	-	0.07	0.07	0.10
Modal damping $\zeta_{5,6...}$	-	0.10	0.10	0.10

Both piers and the Kemi-I steel lighthouse have experienced severe ice-induced vibrations, the latter being in particular very sensitive to vibrations and also suffering structural failures owing to resonant type of ice loading. Resonant behaviour has not yet been recorded with the Kokkola test lighthouse after three months in ice conditions during its first winter of operation.

The superstructures of Kokkola test lighthouse include a special vibration isolation system, /33/, that permits the foundation and superstructures to vibrate independently with only weak interconnection. The vibration isolation system includes rubber shear damping elements that give high internal

damping values. In laboratory model tests equivalent linear damping coefficients of 0.06 for the superstructure motion have been measured. Together with other structural, foundation and hydrodynamic damping, modal damping coefficients greater than 0.07 are feasible. In Kemi-I steel lighthouse and the pier, which have rigid connection between foundation and superstructures, modal dampings starting from 0.03 are reasonable, compare sect. 2.8.

5.2 Stability

In the root extraction method for stability only calculations convergence in QR-algorithm was usually fast and all roots were solved with good numerical accuracy, with relative errors of the order 10^{-9}. In some parameter combinations, however, the solution required more iterations than in the original form of IMSL-procedures. The stability requirement according to the Tondl-method is calculated in the same program as the roots of system of differential equations of motion and no numerical difficulties exist.

The parameters of ice that have an effect on dynamic stability are ice thickness, velocity and the steepness of negative slope in the ice crushing strength curve. In computer analysis the velocity of ice is determined in such a way that the initial stress rate will be that of the steepest descent point. From eq. 3.3 it can be proved that φ is directly proportional to ice thickness and to the second power of ice strength. (The latter is valid if the ice crushing strength curve is scaled only in the σ_c direction while varying ice strength.) In the following only ice thickness is varied; the effect of steepness can then be yielded directly by considering the second power dependence.

The results of dynamic stability analysis for application structures are presented in tables 5.2 to 5.4, where stability according to the Tondl-method and the four lowest natural frequencies of free vibrations are also given. The roots of dynamic equations of motion are so scaled that real parts are relative modal damping coefficients and imaginary parts damped natural frequencies. In an aperiodic case the modal damping coefficient of mode j is calculated from its real roots using the equation

$$\zeta_j = \frac{\lambda_{j1} + \lambda_{j2}}{2\sqrt{\lambda_{j1} \cdot \lambda_{j2}}} \qquad (5.1)$$

which is solved from the definition of roots in an aperiodic case

$$\lambda_{j1,2} = p_j \left(1 \pm \sqrt{1 - \frac{1}{\zeta_j^2}}\right) \qquad (5.2)$$

where p is a constant, compare eq. 3.11 with $\omega = 0$.

Table 5.2 Stability of Kemi - I Steel lighthouse

h	ζ	$\pm if$	ζ_{Tondl}	f_0
10	-0.0173	0.843	-0.0173	0.8428
	0.0238	3.817	0.0237	3.8193
	-0.0404	8.485	-0.0403	8.4972
	-0.0696	12.63	-0.0696	12.663
20	0.0031	0.846	0.0033	
	0.1457	3.796	0.1425	
	-0.0253	8.456	-0.0248	
	-0.0689	12.63	-0.0688	
40	0.0658	0.866	0.0702	
	0.6340	3.197	0.5295	
	0.0080	8.196	0.0260	
	-0.0669	12.62	-0.0664	
70	0.1322	0.980	0.2386	
	3.080	0	1.504	
	-0.0038	7.745	0.1538	
	-0.0650	12.58	-0.0604	
100	0.0818	1.054	0.4879	
	9.248	0	2.9454	
	-0.0209	7.647	0.3429	
	-0.0654	12.55	-0.0516	
140	0.0370	1.073	0.8129	
	17.52	0	4.825	
	-0.0291	7.621	0.5894	
	-0.0662	12.53	-0.0399	
cm	-	Hz	-	Hz

Table 5.3 Stability of a pier

h	ζ	$\pm if$	ζ_{Tondl}	f_0
10	-0.0083	2.938	-0.0083	2.9299
	-0.0174	4.014	-0.0175	4.0189
	-0.0458	10.635	-0.0458	10.644
	-0.0861	14.553	-0.0861	14.609
20	+0.0289	2.997	+0.0317	
	+0.0468	3.978	+0.0424	
	-0.0000	10.659	-0.0013	
	-0.0792	14.548	-0.0788	
40	+0.0122	3.273	+0.1718	
	+0.5339	3.932	+0.2520	
	+0.2598	10.210	+0.1545	
	-0.0574	14.417	-0.0534	
70	-0.0228	3.289	+0.5331	
	5.635	0	+0.7927	
	+0.0545	6.952	+0.5564	
	-0.0553	13.913	+0.0121	
100	-0.0315	3.288	1.0602	
	13.32	0	1.5818	
	+0.0104	6.928	1.1428	
	-0.0641	13.797	0.1077	
140	-0.0356	3.287	1.9802	
	26.31	0	2.9585	
	-0.0924	6.913	2.1661	
	-0.0689	13.757	0.2745	
cm	-	Hz	-	Hz

Table 5.4 Stability of Kokkola test lighthouse

h	ζ	$\pm if$	ζ_{Tondl}	f_0
10	-0.0699	0.431	-0.0699	0.4319
	-0.0700	1.373	-0.0700	1.3764
	-0.0640	4.824	-0.0639	4.8305
	-0.1163	12.334	-0.1164	12.420
20	-0.0698	0.431	-0.0698	
	-0.0699	1.373	-0.0699	
	+0.0027	4.859	+0.0025	
	-0.0913	12.354	-0.0911	
40	-0.0691	0.431	-0.0695	
	-0.0696	1.373	-0.0696	
	+0.2661	5.016	+0.2351	
	+0.0009	12.246	-0.0027	
70	-0.0686	0.431	-0.0685	
	-0.0692	1.374	-0.0688	
	2.609	0	+0.8351	
	+0.0604	9.390	+0.2251	
100	-0.0676	0.431	-0.0671	
	-0.0693	1.375	-0.0676	
	7.767	0	+1.7106	
	+0.0127	9.049	+0.5576	
140	-0.0667	0.432	-0.0646	
	-0.0695	1.375	-0.0656	
	16.88	0	+3.238	
	-0.0401	8.958	+1.138	
cm	-	Hz	-	Hz

In the Tondl-method the effect of internal positive damping, coefficients ζ in table 5.1, are added to the damping requirement of eq. 3.22 so that the presented results are readily comparable with the real parts of corresponding exact roots.

The results for Kemi-I steel lighthouse prove clearly its in-situ observed sensitivity to ice-induced vibrations. Even ice less than 10 cm thick makes the second mode unstable, and thinner than 20 cm also makes the first mode unstable. With ice more than 50 cm thick the second mode will undergo aperiodic divergencies from the static equilibrum position. The measurements in nature /30/ with 10 cm thick ice showed continuous vibration in the second mode. With 55 cm thick ice pure first mode vibrations occurred but more common was a combination of first and second modes simultaneously. This behaviour fits well with the calculated roots.

The stability of the fourth mode appears to be rather insensitive to ice thickness. The same is true of the fourth mode of the pier and with the first two modes of Kokkola test lighthouse.

The sign of real part, stability condition, changes twice with increasing ice thickness with the third mode of Kemi-I, with the first and third mode of the pier and with the fourth mode of Kokkola test lighthouse. The explanation for this phenomenon is the dependence of φ_{nn}-term, eq. 3.3, on pile diameter to ice thickness ratio. As the ice thickness is increased the coefficient κ changes, and, as ice strength is scaled with κ, and, as the velocity of ice is adjusted to keep the initial point at the steepest point in the ice crushing strength curve, φ_{nn} will be then proportional to the second power of κ. Thus the implicit nonlinearities with ice thickness change will also cause nonlinear behaviour in roots. Especially in aperiodic cases it is easy to see the proportionality of real parts of roots to the first power of ice thickness and to the second power of ratio effect κ.

Observations of piers in nature have shown resonant vibrations in both the first and second natural modes. The calculated roots already show instability with ice thinner than 20 cm. Measurements of Kokkola test lighthouse have not yet (20th March -78, first winter of operation) revealed ice-induced vibrations with the first or second modes, which are stable for all ice thicknesses.

The approximative method of Tondl predicts stability conditions excellently for practical design calculations provided that all relative damping coefficients ζ are small, smaller, say, than 0.15. Usually stable modes are predicted correctly although in some other mode a greater real part exists. Modes then predicted as being unstable may, however, be stable. Differences for the exact roots are the greater the greater the unstabilizing effects.

Damped natural frequencies change strongly with ice thickness. First modes seem to have a slightly increasing trend with increasing ice thickness. An intuitive explanation is that negative ice damping accelerates motion and thus increases the frequency. A more usual trend, however, is decreasing frequency, which can be explained by the $\sqrt{1 - \zeta^2}$ effect.

Limit cycle integration, see table 5.6, gave results that also showed stability with 10 cm thick ice for the pier and Kokkola test lighthouse: the initial disturbance decayed exponentially out. In all other cases except with 140 cm thick ice with Kokkola test lighthouse the initial disturbance grew and structure started to vibrate. Limit cycle frequencies are, however, different from those predicted by the imaginary parts of roots, which are valid only for very small vibration amplitudes. The exception of stability prediction for 140 cm thick ice is explained in the discussions of the numerical integration, sect. 5.3.

5.3 Limit cycles

The calculated dynamic response of structure and limit cycles are dependent on both the number of included modes and the time step in numerical integration. The time step was varied in one example to have 20, 50 and 100 steps during the shortest period of included modes. The resulting limit cycle frequency increased from 1.284 to 1.290 and 1.299 Hz respectively. As the truncation error in Runge-Kutta integration is of the order five to time step, Richardson's extrapolation can be used to improve accuracy further. Using the last two values no change in the fourth figure of 1.299 Hz appeared. Using 20 time steps for the shortest period in practical calculations will give errors of 1.2 % in this limit cycle frequency range. It is expected to have still smaller truncation errors with lower frequencies and greater errors with higher frequencies. In each time step case resulting displacement, velocity and acceleration values at the ice action point were almost identical and hence the time step has no significant effect on ice and structure interaction. However, increasing the time step so that less than two time steps were used during the shortest period worsened results considerably.

In order to find out the effect of the number of natural modes included in the numerical integration the pier was analysed by incrementing the number of modes from 1 to 7. Results are presented in table 5.5.

Table 5.5 Effect of the number of modes in numerical integration.

Number of modes	Highest frequency	Relative amplitude	Maximum displ.	Minimum velocity	Crushing frequency
	Hz		mm	cm/s	Hz
1	2.93	0.055	...	...	2.1
2	4.02	0.144	27	-35	1.33
3	10.06	0.287	30	-34	1.30
4	14.6	0.713	31	-35	1.28
5	16.9	0.074	31	-34	1.29
6	21.0	0.275	31	-31	1.34
7	30.0	0.349	31	-32	1.37
10	66.4	-	31	-32	1.39

The maximum displacement at the ice action point does not change any more significantly after 4 modes but minimum velocity during crushing decreases. The frequency response first decreases and later increases with an increasing number of modes. The reason is that if not enough modes are included the behaviour of the response is simpler, which gives an effect similar to damping being greater. This for its part increases frequency, as is found later.

After four modes crushing frequency starts to increase, which is partly due to the decreasing time step and mostly due to faster acceleration to crushing caused by higher modes. It should be noted that acceleration increases but minimum velocity during crushing decreases. The effect of the fifth mode is less pronounced than that of the sixth or seventh modes, which reflects the importance of relative amplitudes of modes at the ice action point. All ten modes together do not improve results significantly when compared to results with seven modes. In practical calculation the utilization of more than seven modes would require denser node meshes than those in fig. 5.1.

Internal damping plays one major role in the dynamic response. If ice thickness is small internal damping may overrule the negative damping effect of ice and limit cycles will have zero amplitudes. If self-excited vibrations arise both their amplitudes and frequencies are strongly dependent on internal damping.

In one test run for Kokkola test lighthouse the relative internal damping coefficients of the third and fourth mode were changed from 0.05 to 0.20 and 0.50. The resulting frequency of limit cycles increased from 1.98 to 2.45 and 3.15 respectively. An approximative upper boundary for the frequency would have been 4.02 Hz according to eq. 5.3, see sect. 5.4. The maximum deflection at the ice action point was reduced only 3 % totally, but the minimum, which was -22 % from the maximum with low damping rose to zero with a damping of 0.20 and to +27 % with a damping of 0.50.

In sect. 2.8 it was stated that ice can also cause positive damping during crushing and grinding of ice into small pieces, while these small pieces are being pushed away, and as the result of friction. Small internal damping gives a response which will have several oscillations before steady deflection grow-up starts. In-situ observations /30/ showed aperiodic damping after crushing and Peyton /40/ also reports great damping. These observations accord much better with the calculated dynamic response with high damping than with low damping. Also the measured saw-tooth like ice force or displacement plots /4, 30, 40/ require more damping in the numerical model than that used in table 5.1. However, the numerical model is as accurate as the ice crushing strength curve used. Alternatively the more pronounced existence of positive damping may be explained better by smaller rather than anticipated negative ice induced damping. The effect of ice temperature should also be considered: according to fig. 2.3 negative damping at -3 ^{o}C is only

about 30 % of that at -10 °C. To be on the safe side in design although the curve in fig. 2.1 does not include any positive ice damping, no positive additional ice induced damping is included until more exact measured ice crushing strength curves are available. The damping coefficients in table 5.1 are therefore also used for limit cycle integration if not otherwise stated.

The developing of limit cycles at ice action nodes in test structures is visualized by plotting out the integrated displacement and force responses as well as phase plane plots in figures 5.2 to 5.10. The ice thickness is the basic varied parameter, but ice strength and damping effects are also shown. In each case five principal modes were included in integration. The typical required Univac 1100 CPU time was 5 minutes for each, the maximum being 20 minutes for low frequency crushing of Kemi-I lighthouse.

Phase plane plots show that limit cycles develop very fast, usually already during the first cycle at the ice action point. Owing to small structural damping and great mass forces, especially in the case of Kemi-I lighthouse, the development of limit cycles at the top of the structure may take tens of cycles. Although at the ice action point the shape of limit cycles is well established, its situation in the phase plane oscillates. With thick ice the ice force is more dominant and then limit cycles become steady sooner.

The most common integrated displacement response is saw-tooth like and this form also appears in ice force plots with thick ice. At the beginning of the cycle the displacement rate is the same or sligthly lower than the initial ice velocity v_0. At the last stage of the displacement grow-up its rate decreases and the point of action in the crushing strength curve moves towards the maximum point. Immediately after this is passed

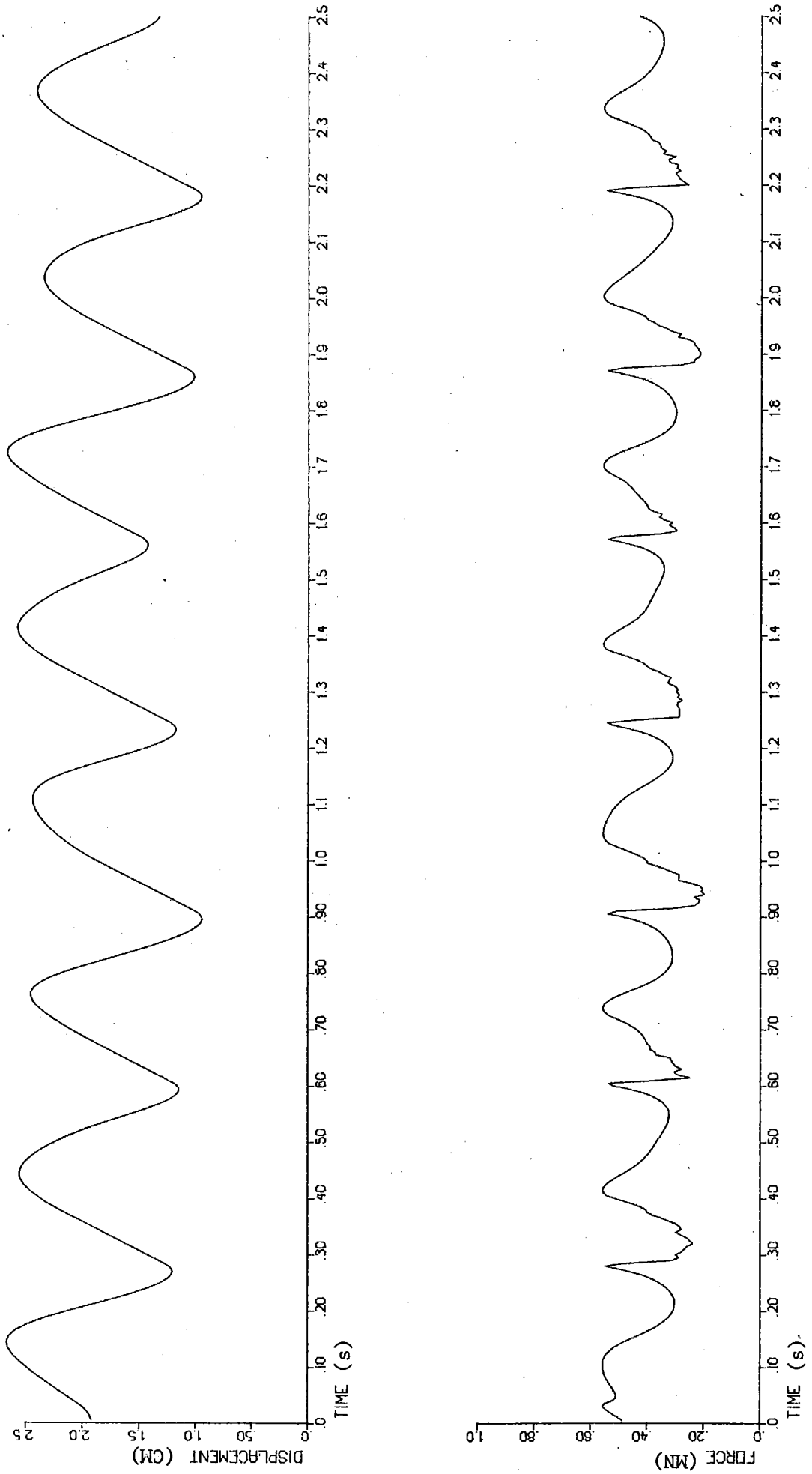

Figure 5.2 a Kemi I, force and displacement plots
h = 20 cm, v_0 = 97,2 mm/s

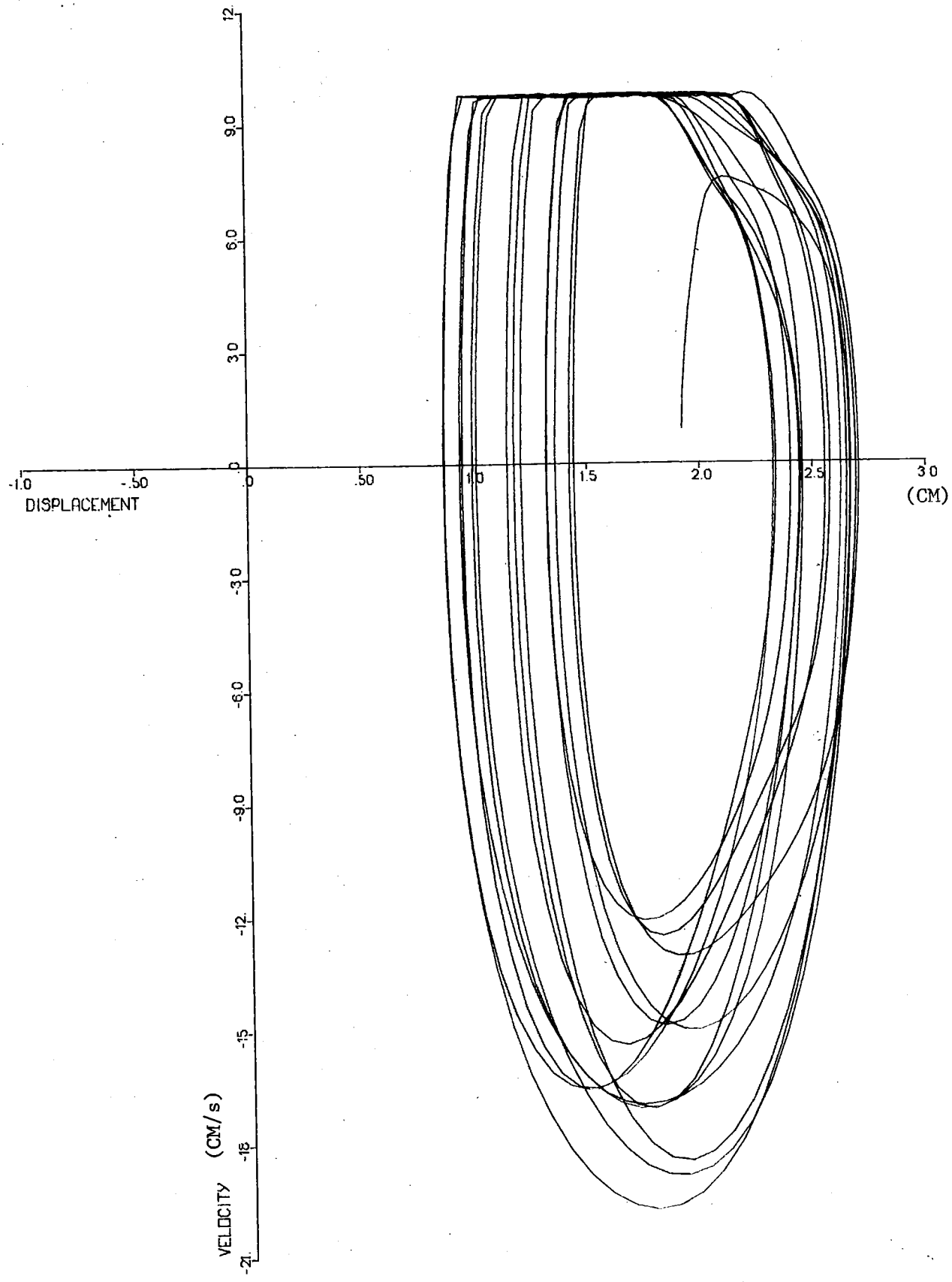

Figure 5.2 b Kemi-I, phase plane plot

h = 20 cm, v_0 = 97.2 mm/s

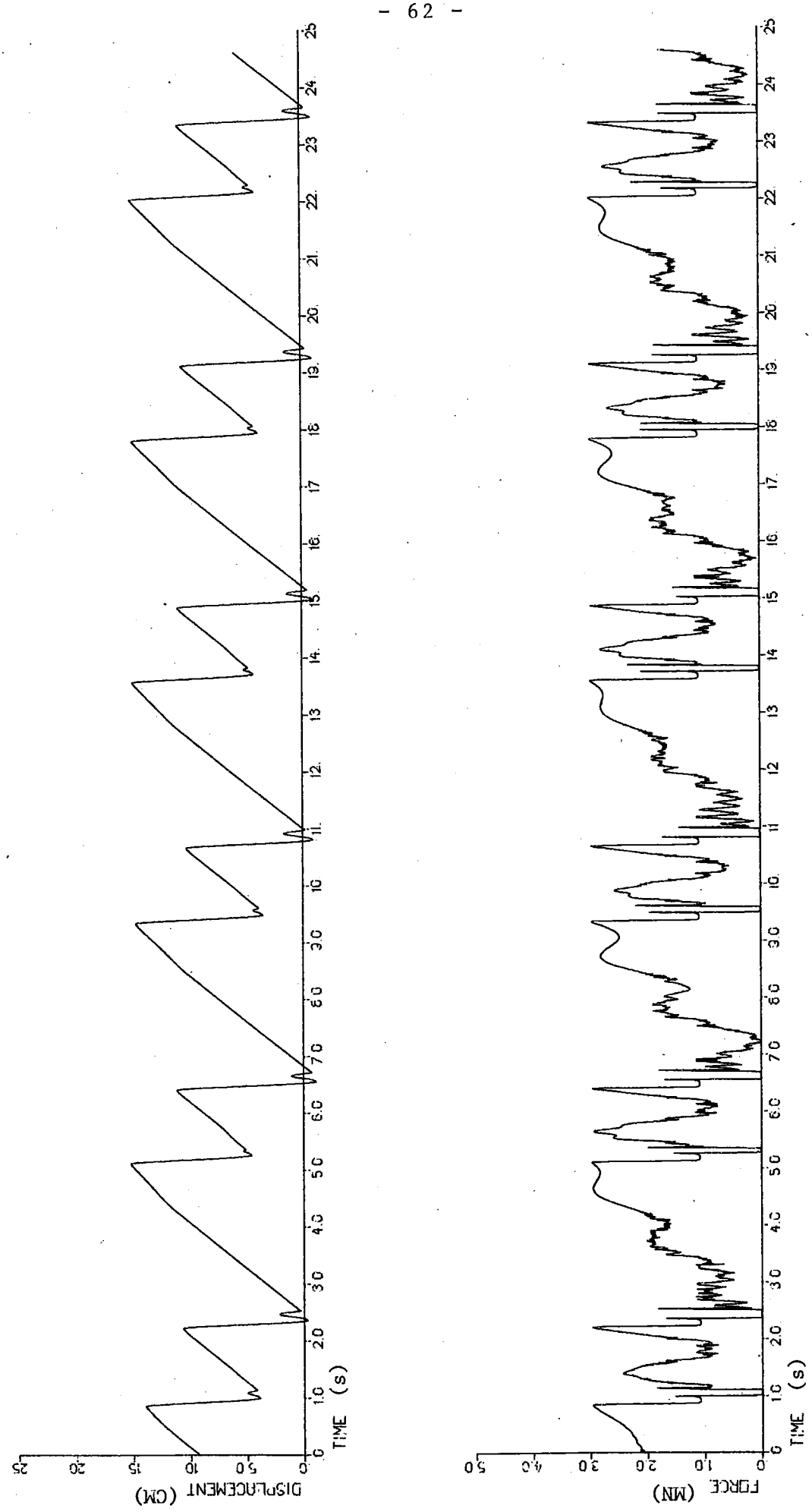

Figure 5.3 a Kemi-I, force and displacement plots
h = 70 cm, v_0 = 64.4 mm/s

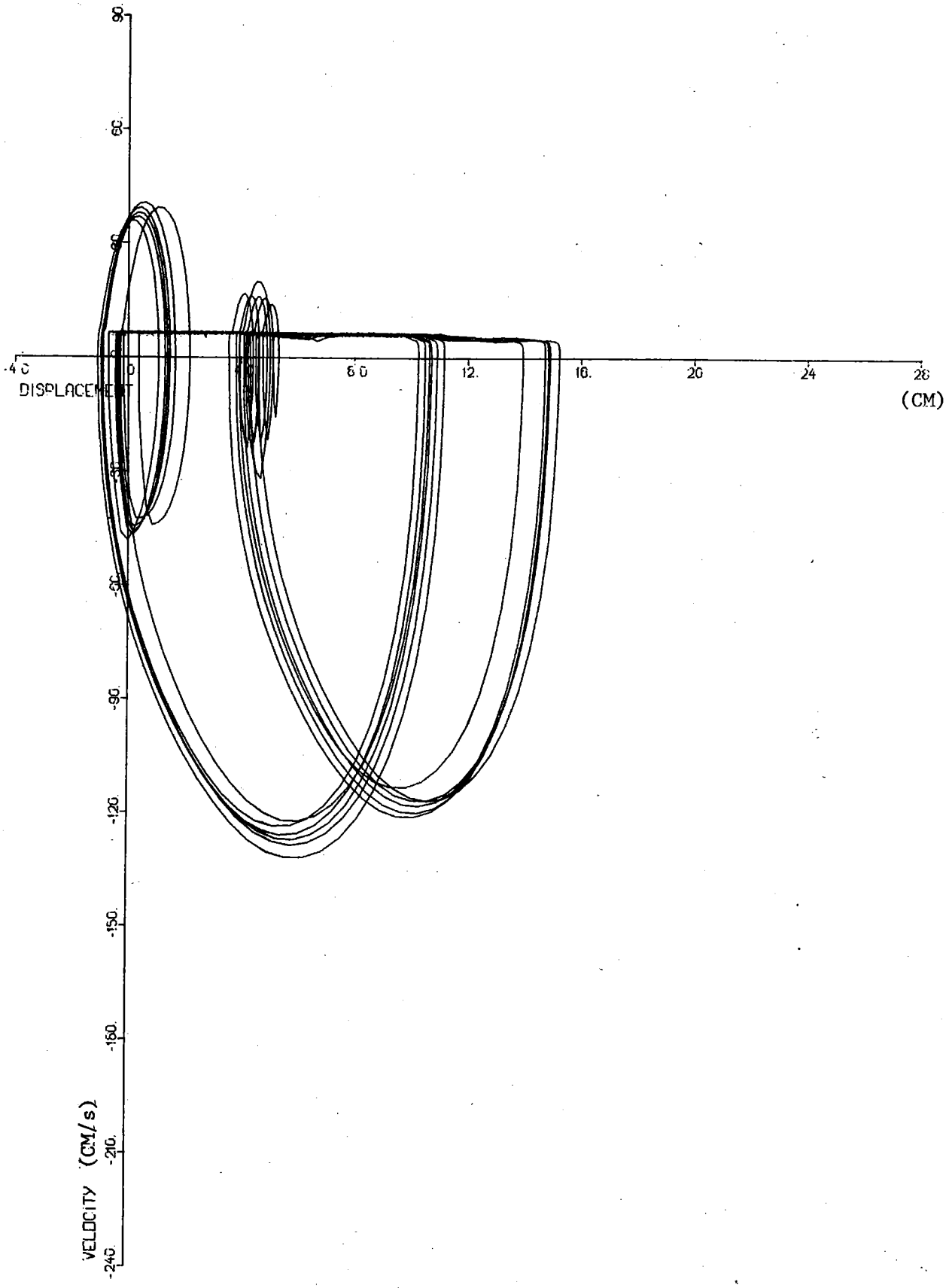

Figure 5.3 b Kemi-I, phase plane plot

h = 70 cm, v_0 = 64.4 mm/s

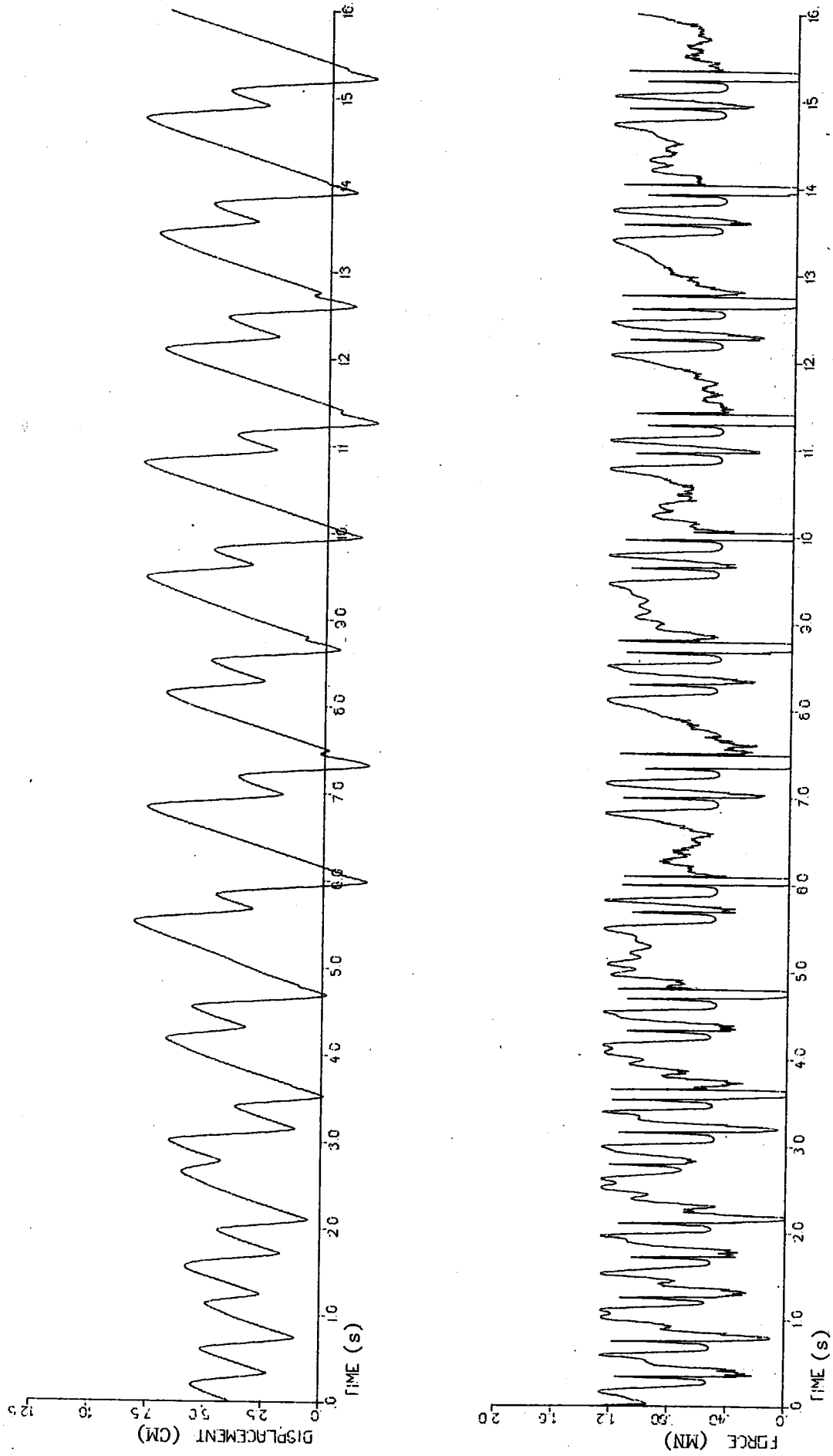

Figure 5.4 a Kemi-I, force and displacement plots
h = 55 cm, v_0 = 118.1 mm/s, σ_c = 1.5 N/mm^2

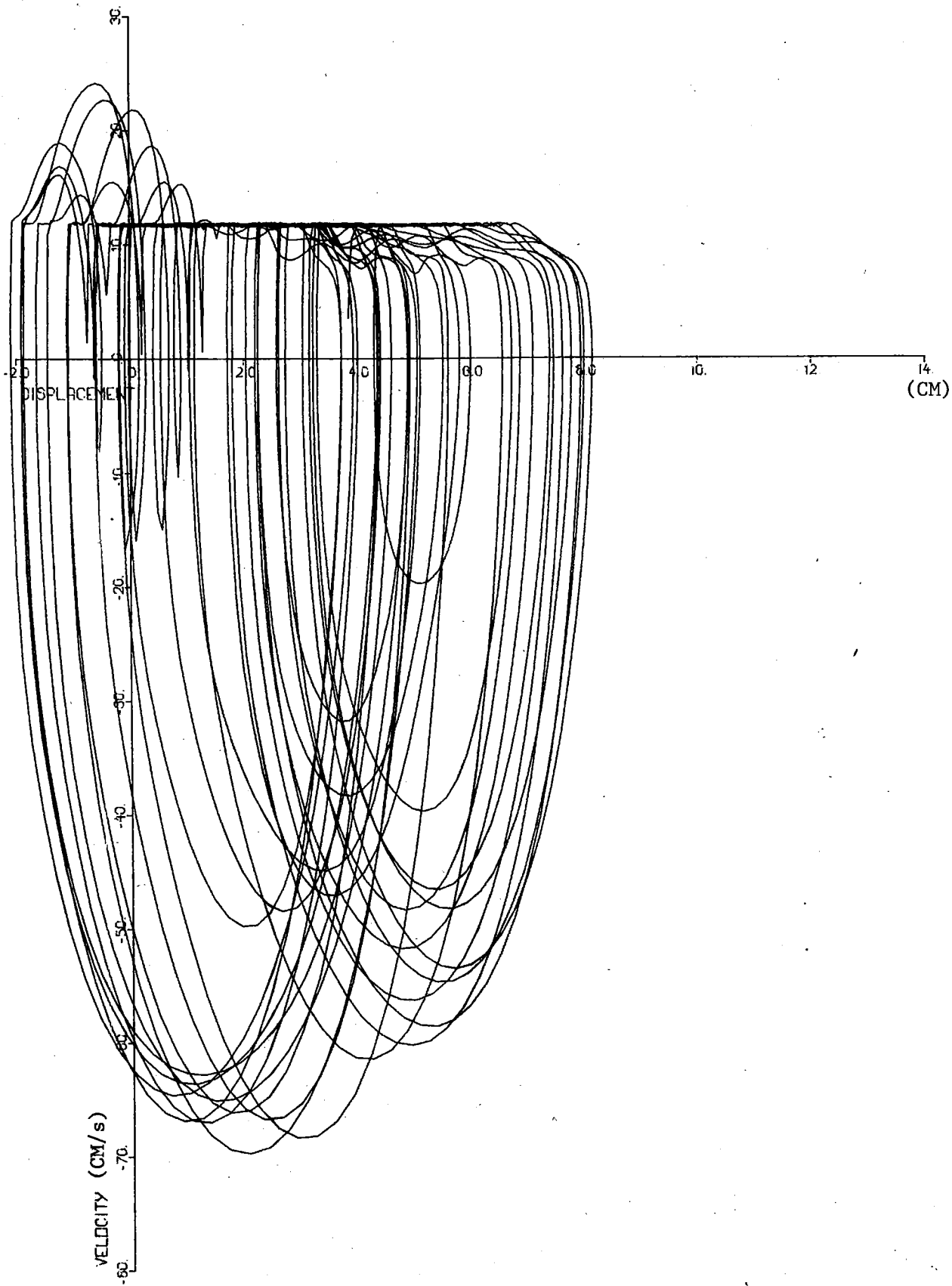

Figure 5.4 b Kemi-I, phase plane plot

$h = 55$ cm, $v_0 = 118.1$ mm/s, $\sigma_c = 1.5$ N/mm^2

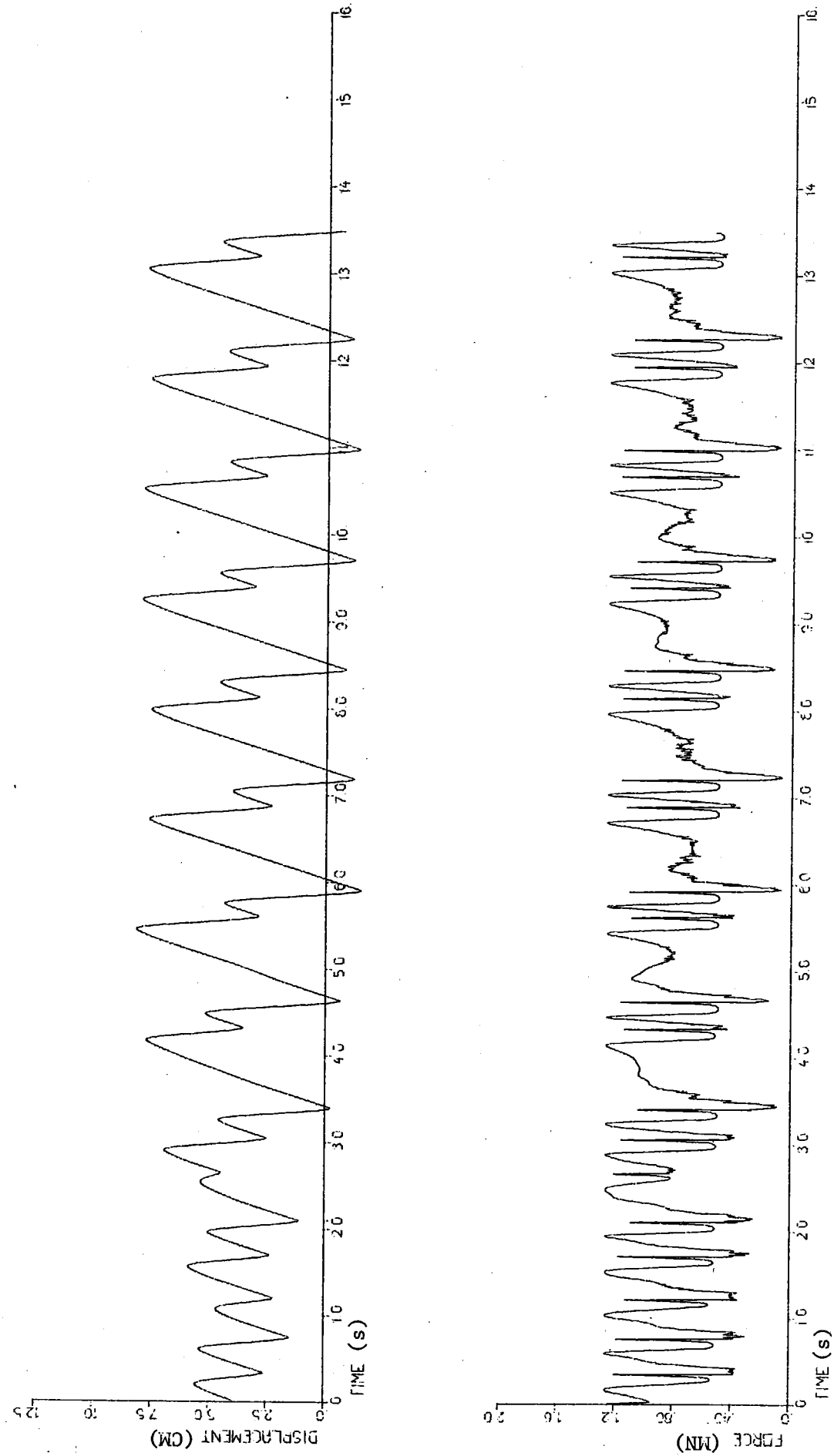

Figure 5.5 a Kemi-I, force and displacement plots
h = 55 cm, v_0 = 118.1 mm/s, σ_c = 1.5 N/mm^2

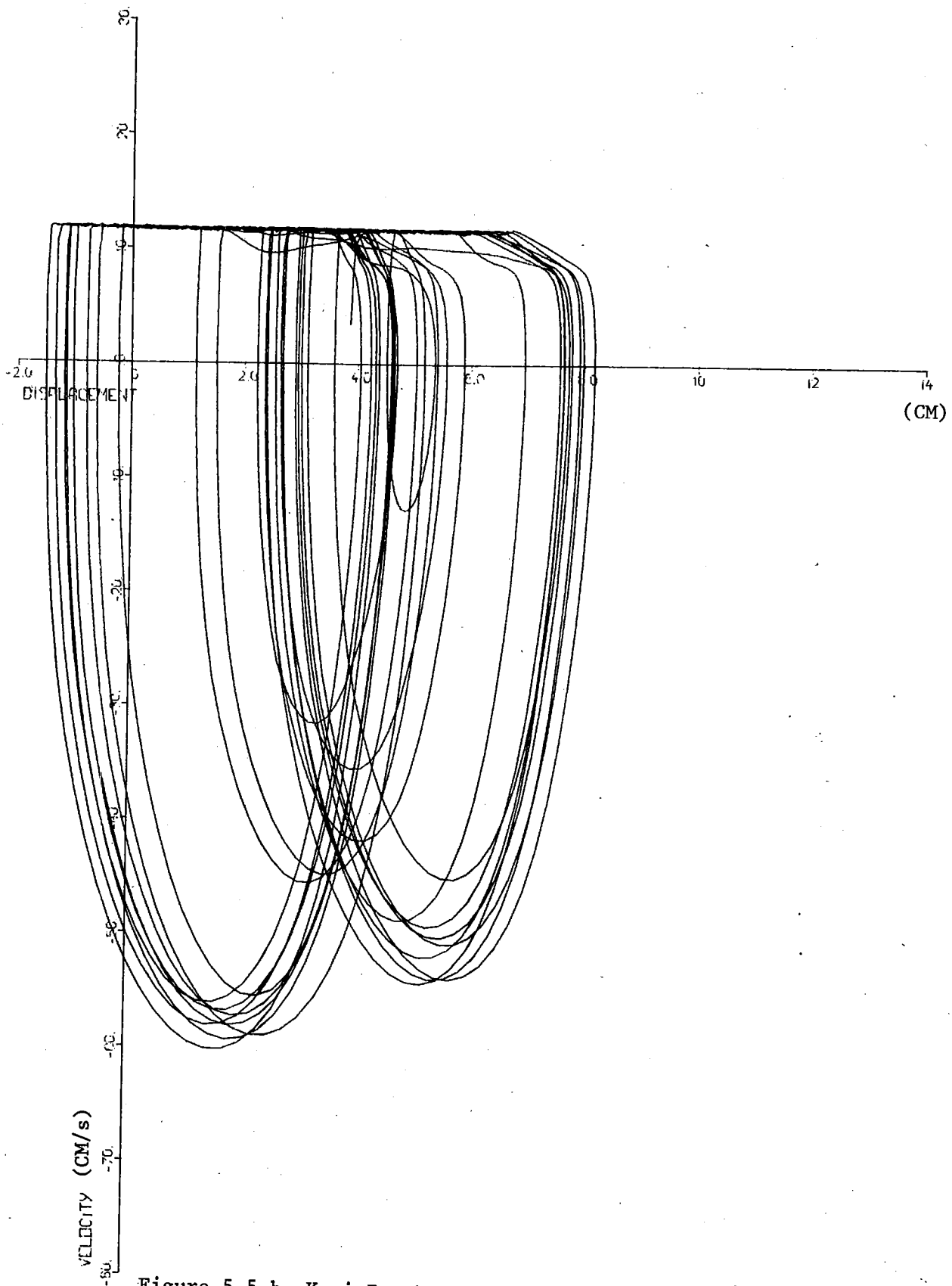

Figure 5.5 b Kemi-I, phase plane plot
h = 55 cm, v_0 = 118.1, σ_c = 1.5 N/mm^2
ζ_i = 0.003, 0.10, 0.15, 0.20, 0.20

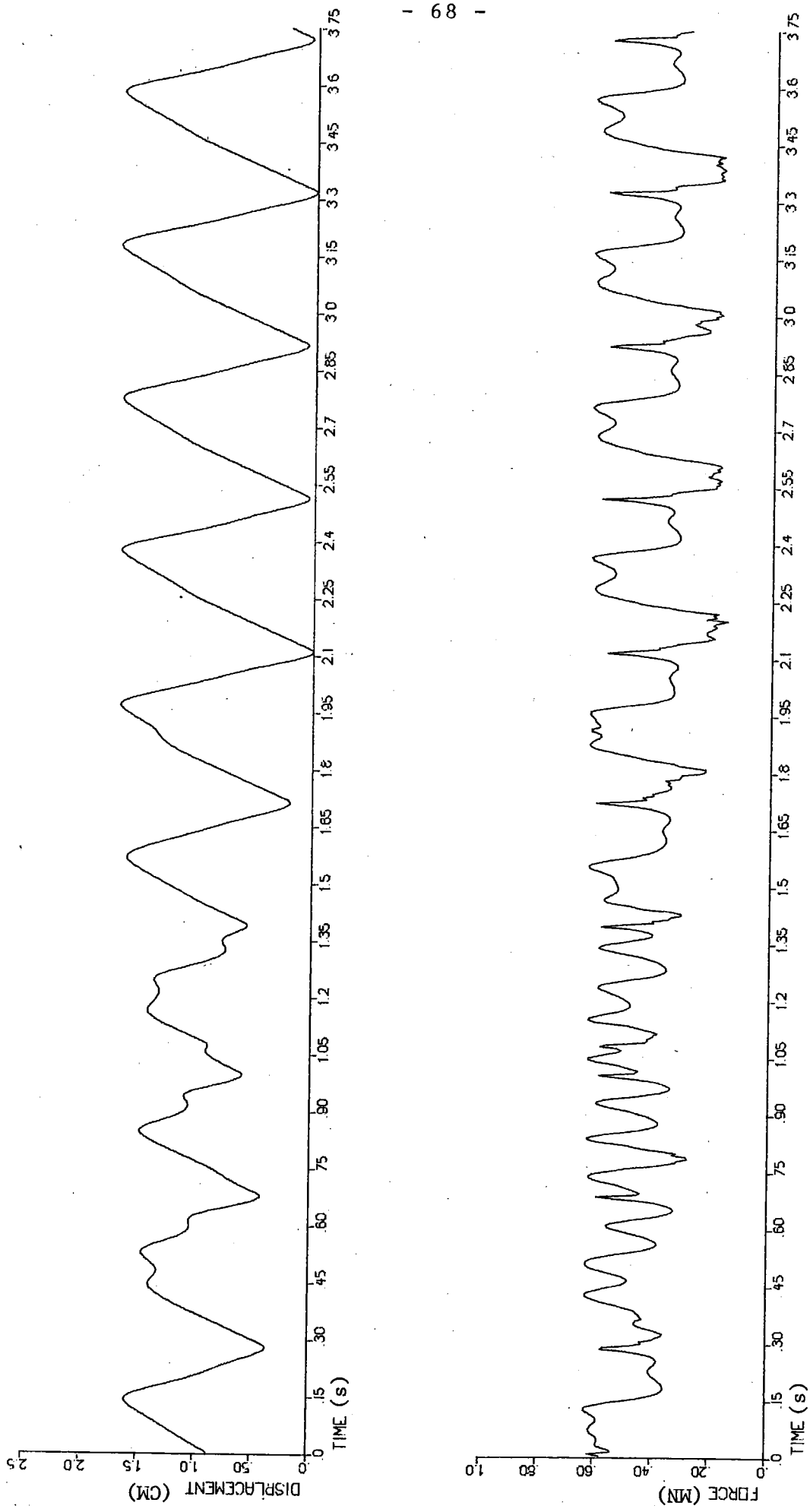

Figure 5.6 a Pier, force and displacement plots
h = 40 cm, v_0 = 75.2 mm/s

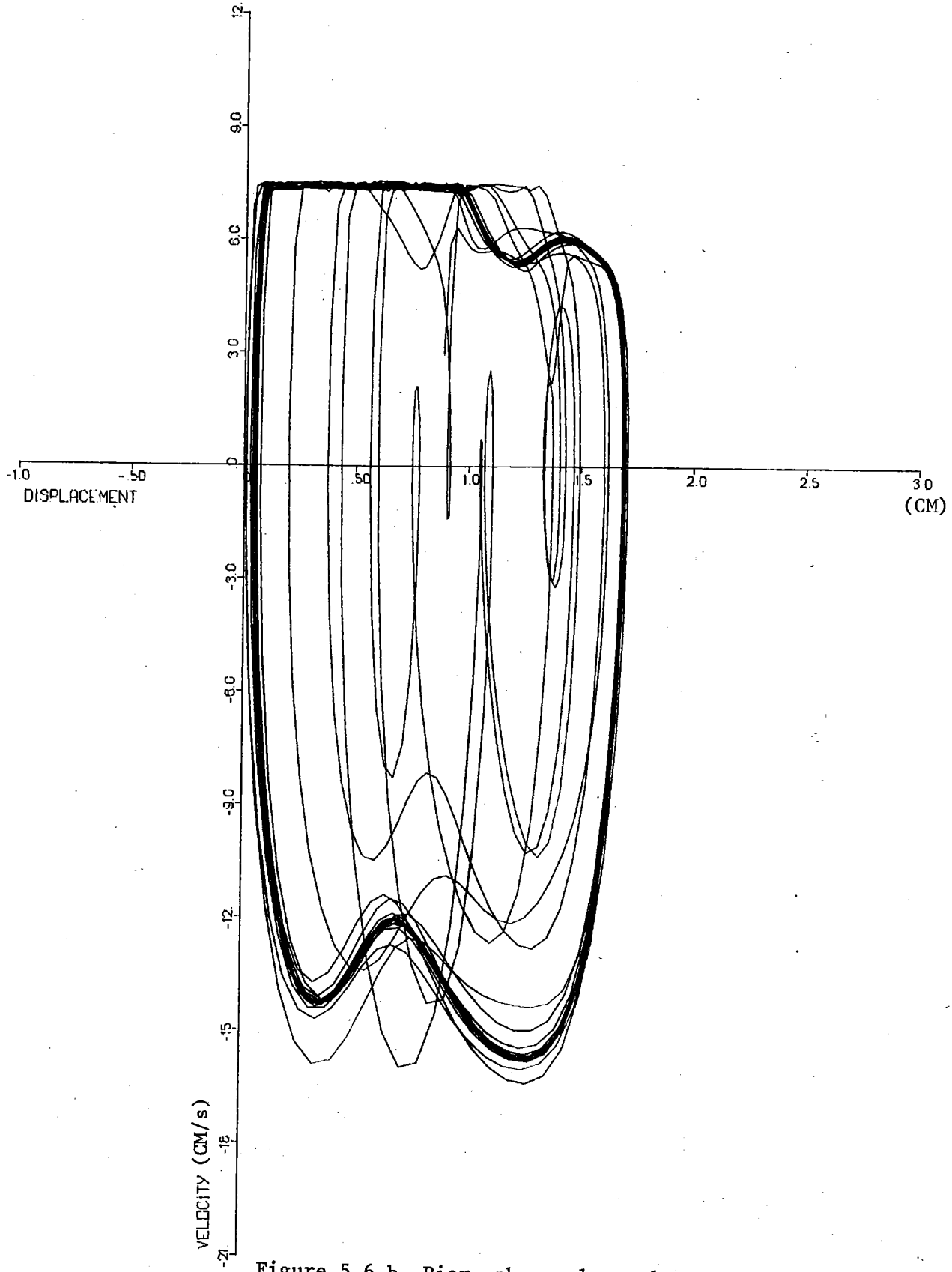

Figure 5.6 b Pier, phase plane plot

h = 40 cm, v_0 = 75.2 mm/s

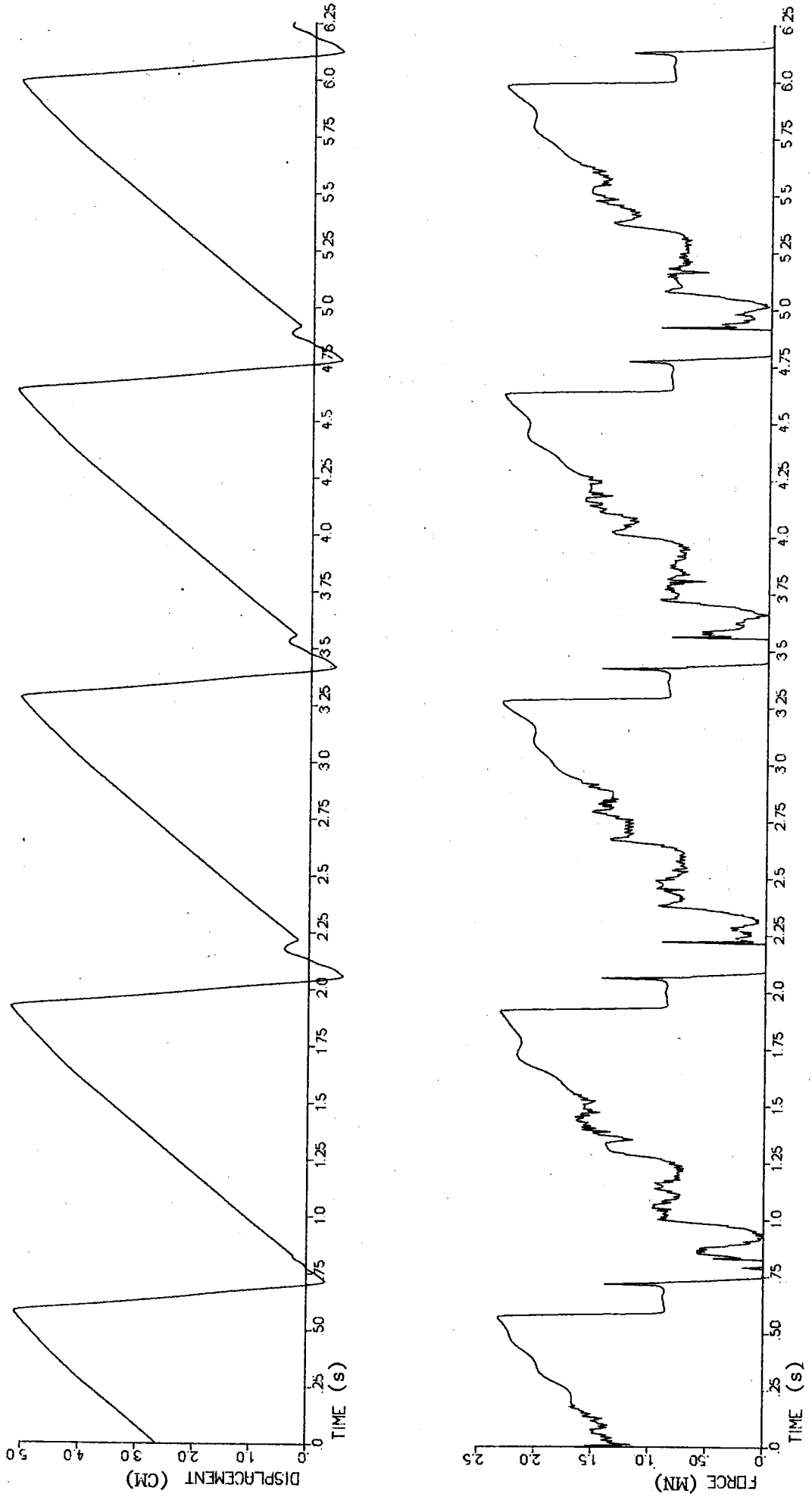

Figure 5.7 a Pier, force and displacement plots
h = 100 cm, v_0 = 51.1 mm/s

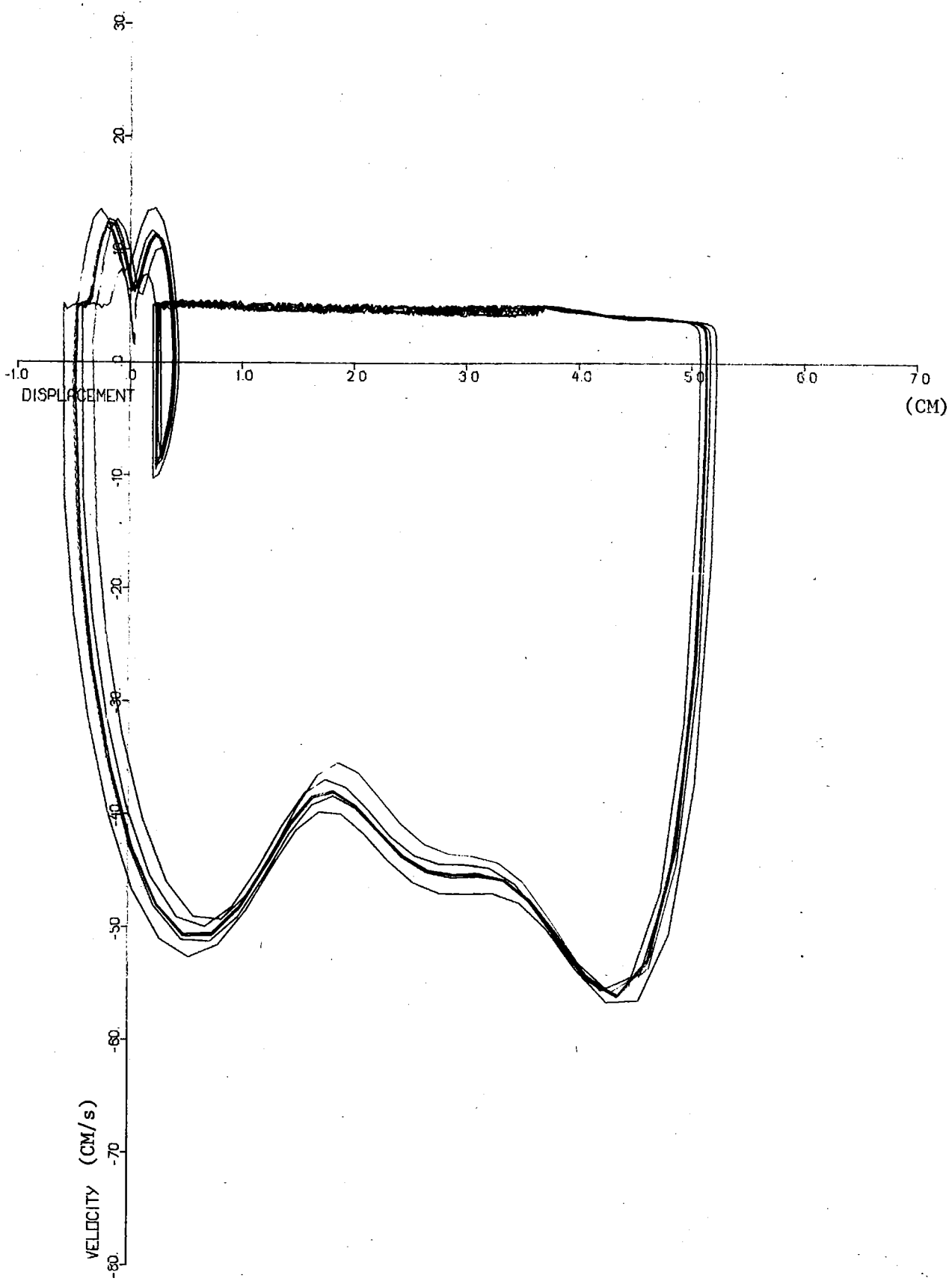

Figure 5.7 b Pier, phase plane plot

h = 100 cm, v_0 = 51.1 mm/s

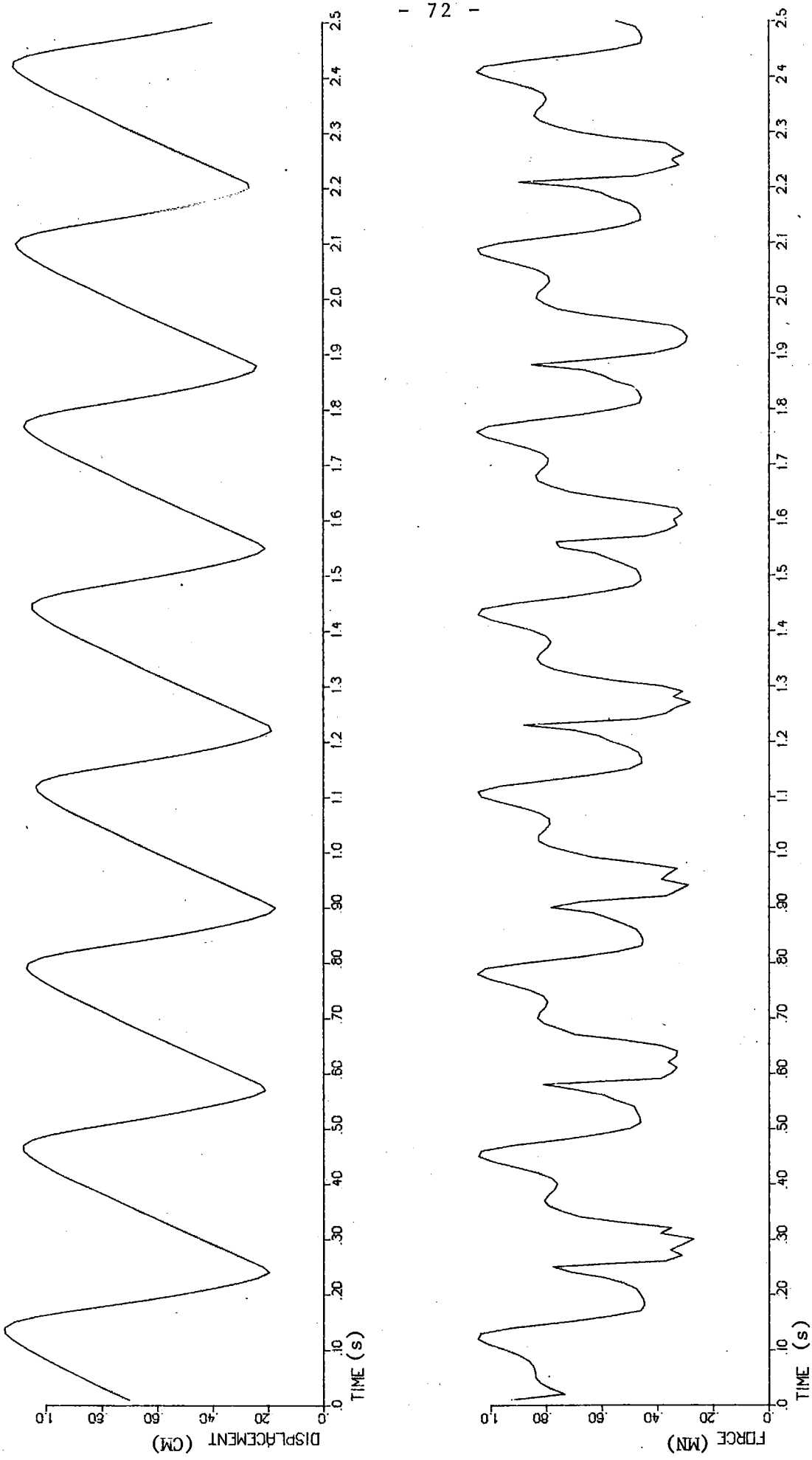

Figure 5.8 a Kokkola test lighthouse, force and displacement plots
h = 40 cm, v_0 = 45.1 mm/s

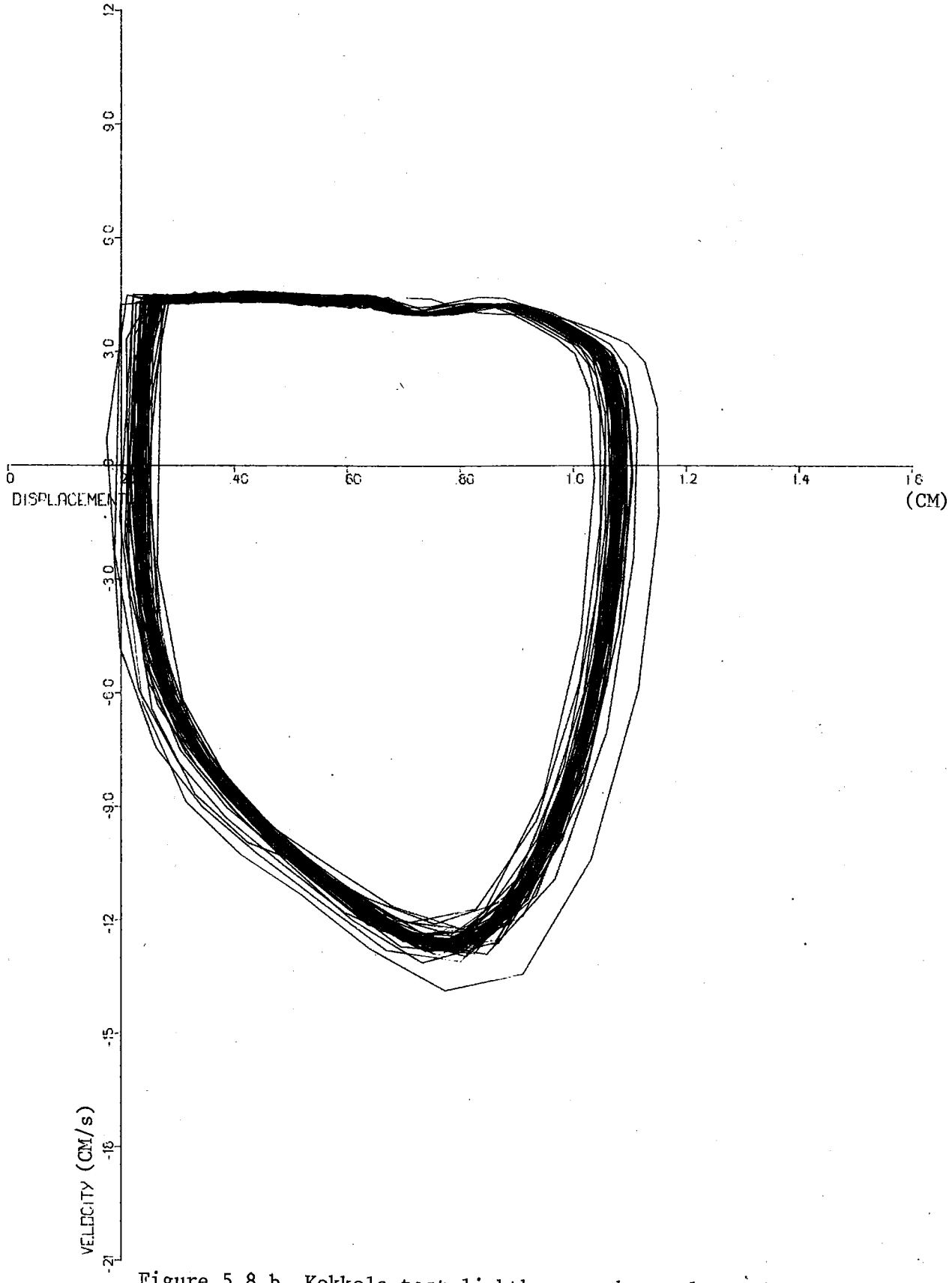

Figure 5.8 b Kokkola test lighthouse, phase plane plot
h = 40 cm, v_0 = 45.1 mm/s

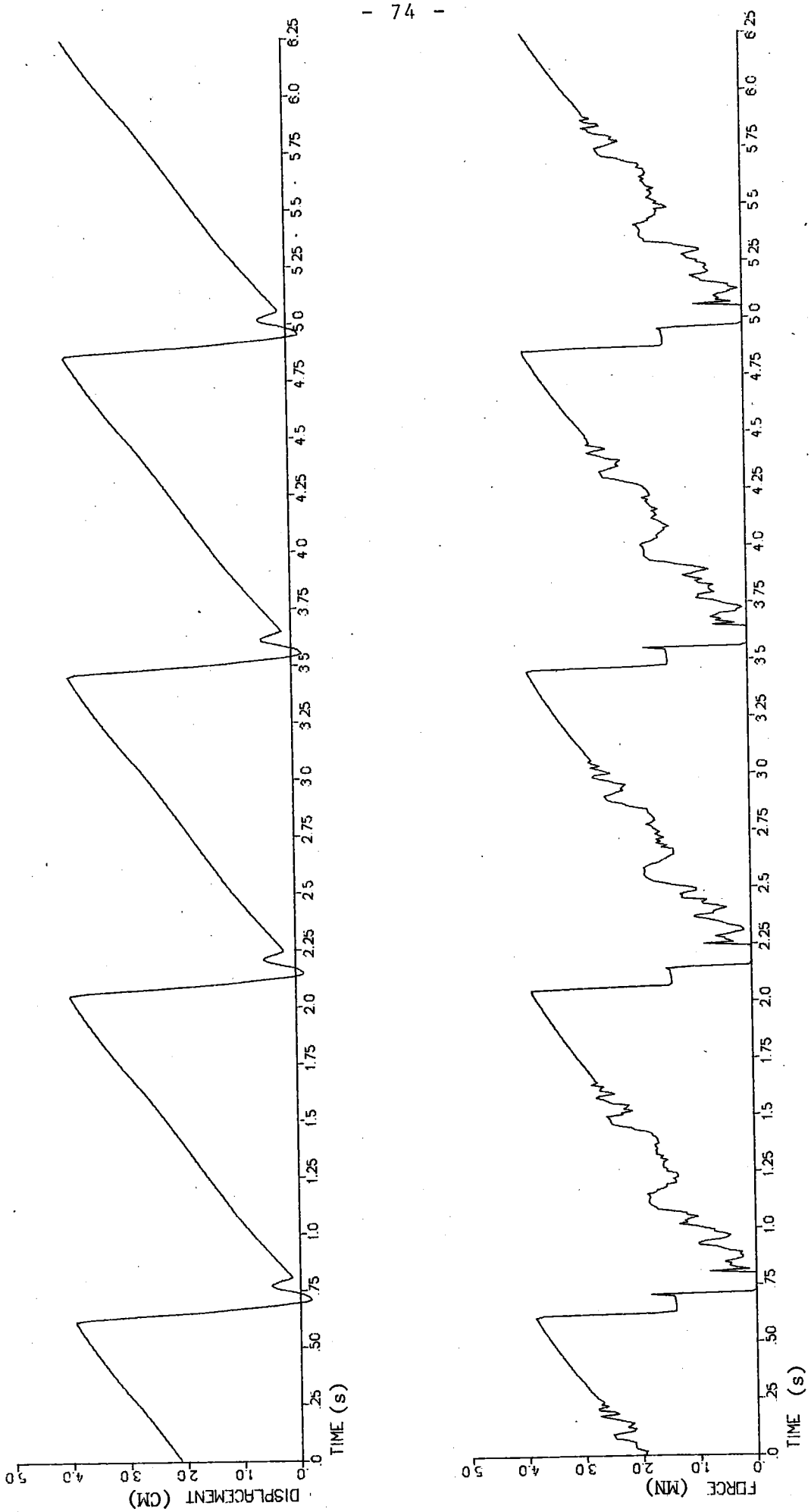

Figure 5.9 a Kokkola test lighthouse, force and displacement plots
h = 100 cm, v_0 = 30.7 mm/s

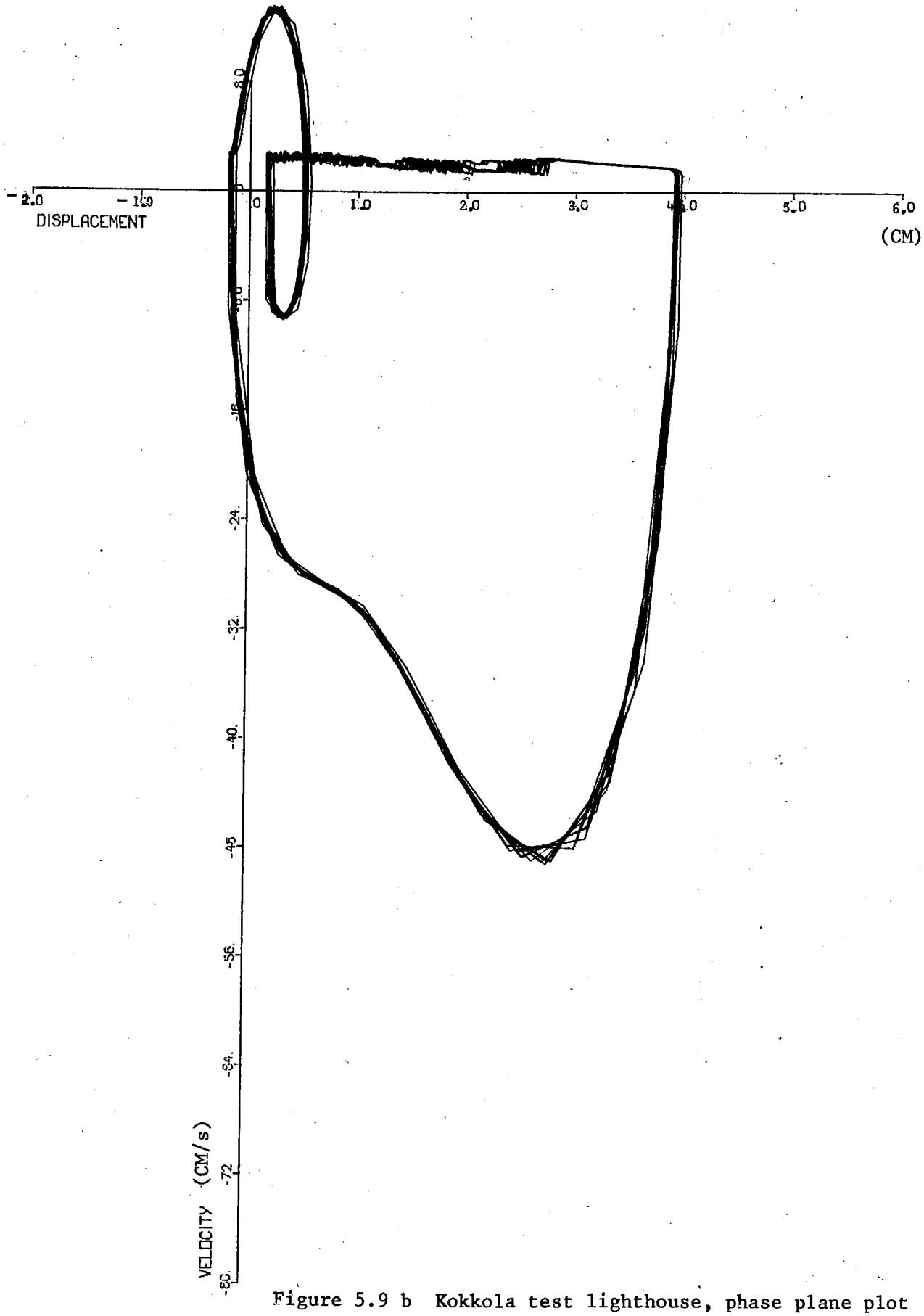

Figure 5.9 b Kokkola test lighthouse, phase plane plot
h = 100 cm, v_0 = 30.7 mm/s

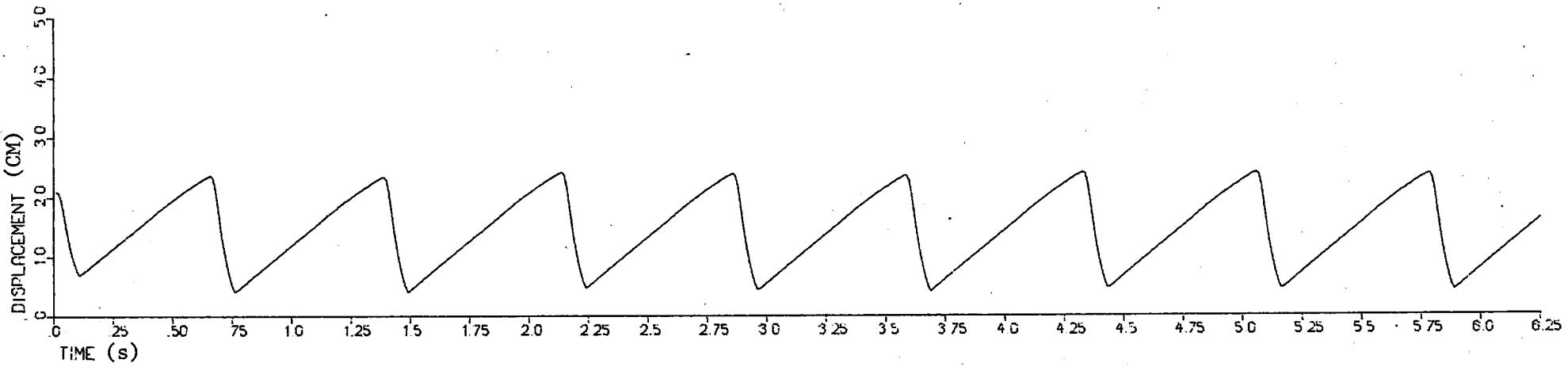

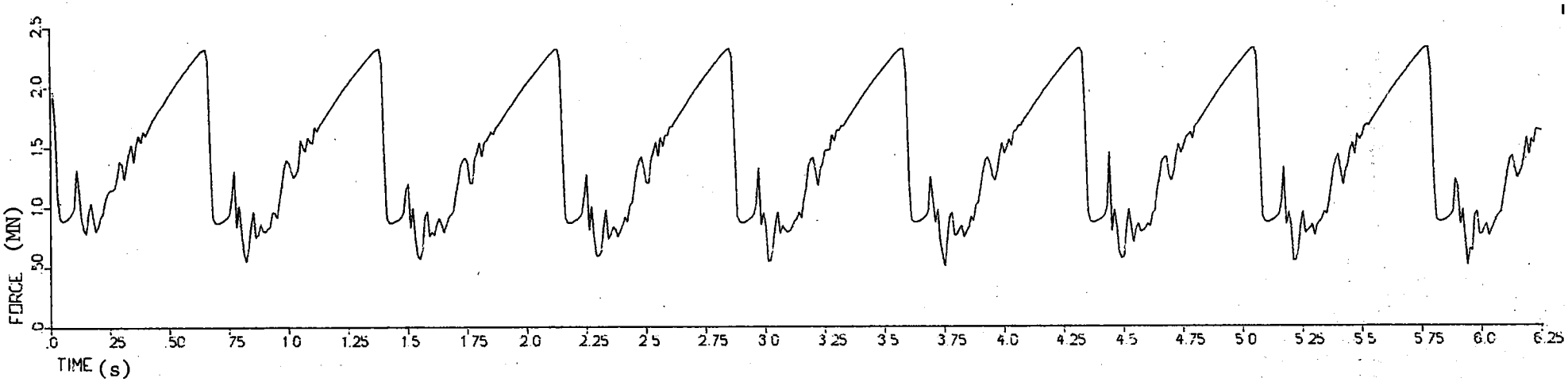

Figure 5.10a Kokkola test lighthouse, force and displacement plots

h = 70 cm, v_0 = 35.7 mm/s

ζ_i = 0.07, 0.007, 0.25, 0.25, 0.25

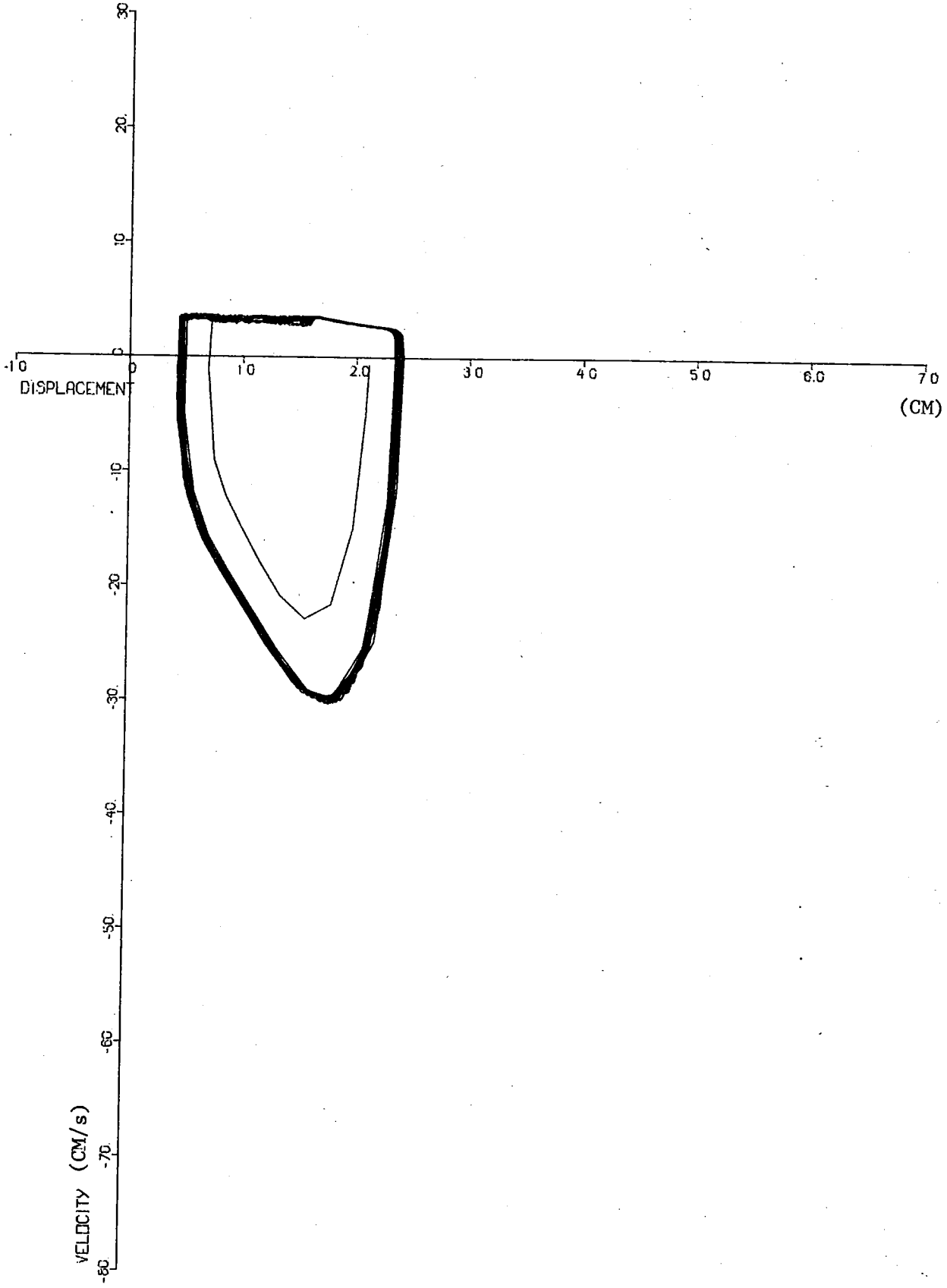

Figure 5.10 b Kokkola test lighthouse, phase plane plot
h = 70 cm, v = 35.7 mm/s
ζ_i = 0.007, 0.07, 0.25, 0.25, 0.25

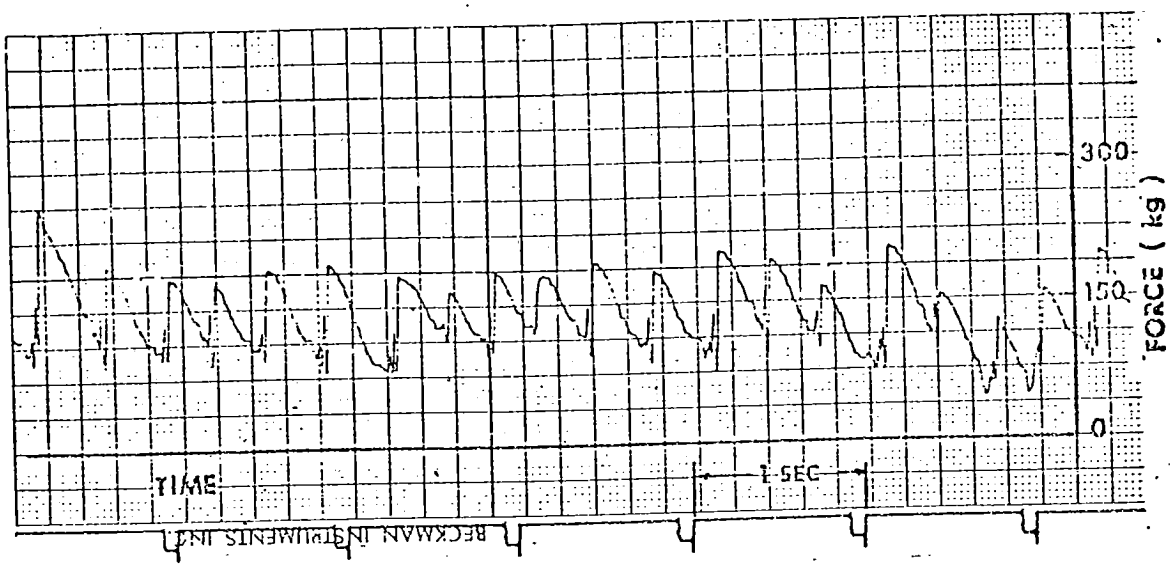

Figure 5.11 Force vs. time record for brittle deformation, Blenkarn /4/.

the crushing and displacement spring-back will start, and the point of action moves in a short time to the brittle, zero slope, region. When the displacement spring-back has ended the point of action returns to the region of low stress rate. During the return phase the maximum point is again passed, which is visible in a peak in the force plot. If displacement spring-back has been great enough, contact between ice and structure is lost. This is common with thick ice and low ice velocity.

Before the next cycle starts and steady contact between ice and structure is established there may be several small hits and spring-backs. If ice induced positive damping is increased the steady contact is achieved earlier. This is observed by comparing fig. 5.4 with 5.5 (or 5.9 with 5.10).

With thick ice and/or low ice velocity the contact between ice and structure is lost and the displacement spring-back passes zero. By decreasing ice thickness or increasing velocity or damping both the displacement and force response curves move to the positive side.

In the case of Kemi-I steel lighthouse a two-stroke crushing phenomenon resulted from the numerical integration with ice thicker than 20 cm, fig. 5.3 to 5.5. The first stroke in crushing occurs mainly with the second natural mode. As the first mode is too slow to follow on, it stops the deflection spring-back at the ice action point, where deflection then starts to grow up again. However, the first crushing has started the spring-back of the massive lighthouse superstructure in the first mode, and after a while the superstructure takes along with it the point of ice action as well and starts the second stroke in the crushing phase. It is noteworthy that exactly similar behaviour was observed with Kemi-I steel lighthouse and a typical double-blow crushing noise heard in-situ, ref. /30/.

The integrated response shows saw-tooth like displacement or ice force plots in low frequency crushing just as observed in nature, /4, 30, 40/. With thinner ice or higher velocities response patterns change, but again the calculated response resembles that observed in nature.

Comparing the computer plot of Kokkola test lighthouse in fig. 5.9 with the measured force history of Blenkarn in fig. 5.11 (time scale from right to left) a good resemblance is observed. It should be noted that Blenkarn's force history measured by strain gauges is not pure ice force but also includes the effects of mass and damping forces. Hence the measured forces do not show zero value at the end of the crushing part, where a zero ice force is predicted by the numerical model. This is typical of all low frequency computer plots and results from the loss of contact between ice and structure after crushing by high modes while the lower modes are lagging. By increasing damping and decreasing ice thickness a still better resemblance is achieved, fig. 5.10; only randomness is absent.

Crushing will occur mostly in a short time after the maximum point in the ice strength curve is achieved, but also on a small scale while the ice force is mounting. This is the result of the contribution of higher modes, which may cause for a short duration the point of action to move right from the maximum point. This is most pronounced with thick ice and at the beginning of a new cycle before deflection grow-up has become steady. This kind of secondary crushing is observed in the unevenness of the ice force plot and in a slower deflection rate than the initial velocity v_0. The effect of secondary crushing can be diminished either by increasing positive internal damping or by decreasing negative ice induced damping.

The exception in the stability prediction for Kokkola test lighthouse with 140 cm thick ice is also the result of secondary crushing. With low ice velocity the secondary crushing is

altogether great enough to dissipate all the initial ice velocity and hence quasi-stable situation occurs. For this case the great internal damping and resulting stable first and second modes are essential. With the pier this kind of situation does not develop although ice thickness is increased up to 170 cm.

5.4 Crushing frequency

During limit cycle integration the appearing frequency of motion in the large is solved as a by-product. With regard to the possiblity of resonance it is important to know if such a combination of ice thickness, strength and velocity exists to give resonant ice forces. In ref. /30, 32/ a simple approximative formula for ice crushing frequency was presented

$$f = \frac{kv}{F_{max}} = \frac{kv}{\sigma_c hd} \qquad (5.3)$$

where k is the lateral stiffness of structure at the point and direction of the ice force.

In numerical integration the dependence of crushing strength on strain rate, polar angle and diameter to thickness ratio are observed, and therefore F_{max} according to eq. 2.11 in denominator should be used in eq. 5.3 when comparing the limit cycle frequency. (In ref. /32/ only constant σ_c value was used). Also the effect of aspect ratio κ on the ice velocity and ice strength must be considered, since numerical integration is carried out in the middle of the descending part of the ice crushing strength curve.

The dependence of the crushing frequency of application structures on ice thickness was analyzed and results are presented in table 5.6 together with the frequency f_0 according to eq. 5.3.

Table 5.6 Limit cycle frequencies

h	Kemi I		The Pier		Kokkola test lighthouse	
cm	f	f_0	f	f_0	f	f_0
10	3.77	9.38	stable	48.7	stable	35.4
20	3.51/0.787	3.59	2.94	17.3	4.72	12.5
40	1.89/0.781	1.19	2.48	5.26	3.01	3.81
70	0.34/0.78	0.445	1.29	1.88	1.09	1.36
100	0.20/0.31	0.231	0.723	0.972	0.490	0.709
140	0.12	0.124	0.346	0.528	stable	0.348

It is observed that in all cases the limit cycle frequency is smaller than that according to the approximative eq. 5.3. The difference is great with high frequency crushing and decreases with thicker ice. After a certain ice thickness the difference again starts to increase. The phenomenon is visualized in fig. 5.10, where ratios f/f_0 are plotted.

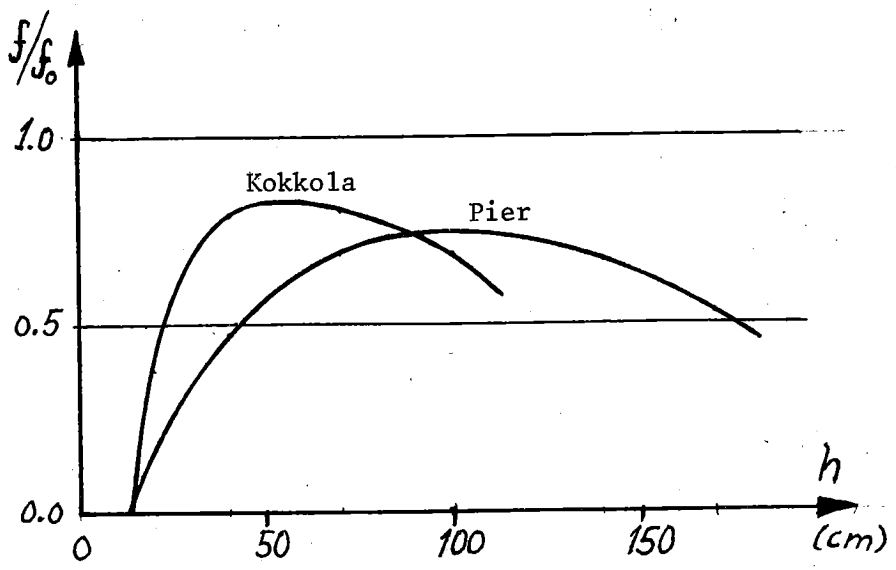

Figure 5.10 Frequency ratio f/f_0 versus ice thickness

As was explained in the previous section secondary crushing will cause lower deflection rates and thus lower limit cycle frequencies. Part of the decrease in frequency is due to

the integration time step and number of modes effect, sect. 5.3, and partly due to a deflection spring back phase which is not included in eq. 5.3. For instance with the pier main crushing - deflection spring back - takes about 11 % of the time of the total period with 100 cm thick ice and about 35 % with 40 cm thick ice. If a deflection spring back phase is observed in eq. 5.3 and more positive damping included or a higher ice temperature considered in limit cycle integration, the limit cycle frequencies calculated in both methods will approach each other quite closely in normal ice thickness reqion with the pier and Kokkola test lighthouse.

The effect of ice velocity was checked for the pier by varying the initial ice velocity from 1/3 to 4 times from the velocity 5.95 cm/s that corresponds to the steepest point in the ice crushing strength curve, table 5.7.

Table 5.7 Crushing frequency dependence on velocity

v cm/s	f Hz	f_0 Hz
1.98	stable	0.626
3.97	0.92	1.26
5.95	1.29	1.88
8.93	1.89	2.82
11.90	2.27	3.76
17.86	2.43	5.65
23.81	2.84	7.53

The lowest velocity is a little way on to the positive slope side in the ice crushing strength curve, and although the initial disturbance was great enough to move the point of action beyond the maximum point at 2.45 cm/s to the negative side, negative damping was not sufficient to sustain vibrations and amplitudes decayed to zero. The two highest velocity values are in the

brittle region ($v_0 > 17.4$ cm/s), but as the zero slope has only a neutral effect autonomous oscillations will receive enough energy from the negative slope region to offset the dissipation of positive internal damping per cycle and thus limit cycles may develop. It is necessary, however, that the initial disturbance moves the point of action sufficiently far to the negative slope region.

Crushing frequency increases with increasing velocity but in general more slowly than eq. 5.3 supposes. The reason is that in addition to those decreasing effects described for table 5.6 additional decrease now occurs owing to moving out from the most favourable point in the crushing strength curve. However, if the change between nearby velocity values in the middle region is considered, eq. 5.3 predicts the change pretty well. In the example an increase in velocity of 1.5 times from 5.95 cm/s increases the crushing frequency only 2.3 % less in numerical integration than predicted by eq. 5.3.

The effect of the ice crushing strength on crushing frequency can be considered by comparing a similar change in ice strength to that caused by the change of ice thickness together with the ratio effect κ^2. Thus the results given in table 5.6 can be interpreted for ice strength by substituting

$$\sigma_{c1} = \sigma_c \cdot \frac{h}{h_1} \cdot \left(\frac{\kappa}{\kappa_1}\right)^2 \qquad (5.4)$$

For instance, changing thickness from 40 to 70 cm corresponds to a change in crushing strength 2.80 times greater in the pier. This is valid in both numerical integration and eq. 5.3. A change in the diameter of the structure does not have any effect in either method.

Kemi-I steel lighthouse had very massive superstructure and flexible foundations. In this case mass forces will become

significant when compared to ice forces and thus eq. 5.3 fails to predict crushing frequencies. However, the trend is a decreasing one with increasing ice thickness as with the other structures and with thick ice results are acceptable. The highly unstable second mode tends to superimpose on the first with ice thinner than 40 cm, and up to 70 cm thick ice if maximum ice crushing strength is reduced to 1.5 N/mm^2. Thus the calculated double frequency crushing also tallies with observed crushing behaviour.

Considering the applicability of eq. 5.3 for practical crushing freqyency prediction, it can be concluded, that it gives correctly the trend for each parameter. The actual frequency (numerical integration) will be about 20 to 30 percent too high at the most favourable action point in the ice crushing strength curve and differences increase if the point of action is somewhere else. However, if positive internal damping is increased or steepness of descending part of the crushing strength curve decreased the difference becomes still smaller. Where mass forces of superstructure are pronounced, eq. 5.3 fails. As for the range of possible ice velocities and thicknesses in nature, eq. 3.5 is handy for predicting whether resonant ice forces are to be expected.

Equation 5.3 or the results of numerical integration also explain the findings of Gaither /11/, who says that the frequency of ice crushing is not dependent on the natural frequency of the structure. This was observed in his laboratory tests while changing the natural frequency of a structure by changing its mass. Because eq. 5.3 does not contain mass terms there will likewise be no change in ice crushing frequency when inertial effects are small and other parameters are kept constant. A change in natural frequency by changing the stiffness would have given a different dependence on the natural frequency.

There is no evidence in the numerical results that ice may have a characteristic frequency of about one cycle per second, as proposed by Peyton /40/ and supported by Neill /35/. On the other hand the frequency, the result either of numerical integration or eq. 5.3, clearly depends on both ice properties: thickness, crushing strength, temperature and the shape of the crushing strength curve, and on structure properties: stiffness, mass and damping distributions. Neill's explanation of the constant size fragements in breaking can be regarded as correct provided that the size of fragments is determined not only by ice properties but also by the structure properties in the interaction.

The omission of elastic ice deformation, sect. 2.6, required the deflection of structure to be great enough. With thinner ice the deflection of structure decreases and hence that supposition is not so well satisfied. For this reason and owing to the greater requirement of modes to be included in numerical integration the previous results with thin ice should be regarded only as trend-giving. The omission of viscoelastic behaviour of ice reduces accuracy in results with frequencies lower than 0.5 Hz.

6 SUMMARY

The presented model for ice and structure interaction observes the effects of ice properties in continuous crushing through the ice crushing strength versus loading rate curve. Average ice properties are used through the thickness of ice and viscoelasticity and random variations are omitted. Restricting considerations to only those cases in which the elastic deformation of ice can be neglected, when compared to the deflection of structure at the ice action point, the dynamic equations of motion are required only for the structure. The structure is discretized using conventional beam finite element techniques. Damping is linearized and modal damping presentation is used.

With the created model three different marine pile structures at the Gulf of Bothnia were analyzed. Although the foundation of the model was ice crushing strength versus loading rate curve measured from the Cook Inlet ice the model predicted the existence of dynamic instability and limit cycles like those observed in nature. Also similar ice force plots were calculated as measured at the Cook Inlet.

The conformity of calculated and measured saw tooth-like ice force and displacement histories offers the best evidence for its part that the basic model is correct for the ice and structure interaction. This makes it possible to test the effect of different ice and structure parameters on the interaction phenomena. The qualitative effect of ice thickness, strength and velocity is given for the application structures.

Quantitative results were also given, but it must be emphasized that their accuracy is dependent on the accuracy of the initial ice crushing strength curve. Total damping has a great effect on quantitative results. Not enough information is available to judge the correct amount of total damping, which is the sum of positive internal structural damping including hydrodynamic effects, positive damping effects in ice crushing and the negative damping due to decreasing crushing strength versus loading rate. Quantitative results should therefore be considered only as rough estimates until more accurate ice crushing strength curves and damping details are available.

Two simple formulas were given for practical ice and structure interaction engineering problems. With the extension of the Tondl-method it is possible to predict the stability of natural modes and with a simple formula the frequency of limit cycles. The reasonable accuracy of formulas was verfied by the analytically exact root extraction method and by numerical integration.

To refine the model requires a test series for more accurate crushing strength curves and to separate positive and negative ice damping effects from the damping of structure. This requires measurements in continuous crushing conditions. An understanding of the qualitative effects of different parameters makes it easier to analyze the results of measuring. The effect of aspect ratio κ can also be tested more accurately than before, since according to the present model it will have second power dependence on ice thickness in the crushing frequency.

The elastic deformation of ice can be taken into account by forming and solving simultaneously the dynamic equations of motion for the ice sheet, too. It will then be possible to analyze ice interaction with structures which are very stiff or large in diameter for which the omission of elastic deformation of ice is no longer justified. The results for the structures analyzed here with thin ice can then be further refined.

Once the model is more refined the always present random variations in physical ice properties should be considered. In numerical integration it would be easy to vary ice crushing strength or thickness randomly, for instance by the Monte-Carlo method, but this would require hundreds of cycles being integrated for the statistical picture of response.

Even its present form the mathematical model described here makes it possible to design structures that are more secure against dynamic ice forces. The Kokkola test lighthouse is an example of a structure in which this method is successfully used. However, conservative safety factors in damping should be utilized until more accurate damping and crushing strength data is available.

REFERENCES

1 Afanas'yev V.P. & Dologopolov I.U. & Shvayshteyn Z.I.: Ice Pressure on Separate Supporting Structures in the Sea, Draft translation 346, CRREL, Hanover, 1972.

2 Andronov A. & Vitt A. and Khaikin S.: Theory of Oscillators, Pergamon Press, Oxford 1966.

3 Assur A.: Forces in Moving Ice Fields, POAC-71, Technical University of Norway, Trondheim 1971.

4 Blenkarn K.A.: Measurement and Analysis of Ice Forces on Cook Inlet Structures, Offshore Technology Conference, Dallas, Texas, 1970.

5 Croasdale K.R. & Morgenstern N.R. & Nuttal J.B.: Indentation Tests to Investigate Ice Pressures on Vertical Piers, Symposium on Applied Glaciology, Cambridge, September 1976.

6 Danys J.V. & Bercha F.G.: Determination of Ice Forces on a Conical Offshore Structure, POAC-75, University of Alaska, Fairbanks 1975.

7 Dunne M. & Noble P. & Edwards R.Y. jr. & Pellegrin C.: Results of Full Scale Ice Impact Load Studies Abroard C.C.G.S Norman McLeod Rogers, POAC-77, Memorial University of Newfoundland, St John's, 1977.

8 Edwards R.Y. & Croasdale K.R.: Model Experiments to Determine Ice Forces on Conical Structures, Symposium on Applied Glaciology, Cambridge, September 1976.

9 Frederking R. & Gold L.: Ice Forces on an Isolated Circular Pile, POAC-71, Techincal University of Norway, Trondheim 1971.

10 Frederking R. & Gold L.: Experimental Study of Edge Loading of Ice Plates, Canadian Geotechnical Journal, Vol 12, No 4, November 1975.

11 Gaither W.S.: Ice Forces on Marine Structures, Proc. IAHR Symposium on Ice and its Action on Hydraulic Structures, Reykjavik 1970.

12 Girkmann K.: Flächertragwerke, Springer Verlag, Wien, 1956.

13 Gold L.W.: Ice - Challenge to the Engineer, Proc. Fourth Canadian Congress of Applied Mechnics, NRC Technical Paper No 395, Ottawa 1973.

14 Gold L.W.: The Failure Process in Columnar-Grained Ice, NRC Technical Paper No 369, Ottawa 1972.

15 Gold L.W.: Engineering Properties of Fresh-Water Ice, Symposium of Applied Glaciology, Cambridge, September 1976.

16 Haynes F.D. & Nevel D.E. and Farrell D.R.: Ice Force Measurements on the Pembina River, Alberta, CRREL Technical Report 269, Hanover 1975.

17 Haynes D.F.: Effect of Temperature and Strain Rate on the Strength of Polycrystalline Ice, CRREL, Hanover, January 1977.

18 Hirayama K. & Schwartz J. and Wu H-C.: Model Technique for the Investigation of Ice Forces on Structures, POAC-73, University of Iceland, Reykjavik 1973.

19 Hirayama K. & Schwartz J. and Wu H-C.: Ice Forces on Vertical Piles: Identation and Penetration, Proc. Third International Symposium on Ice Problems, IAHR, Hanover, New Hampshire 1975.

20 Henry R.F. and Tobias S.A.: Modes at Rest and Their Stability in Coupled Non-Linear Systems, Journal of Mechanical Engineering Science, Vol 3 No 2, pp 163-173, 1961.

21 Hilaire A.O.: Analytical Prediction of the Non-Linear Response of a Self-Excited Structure, Journal of Sound and Vibration, (1976)47(2)185-205.

22 IMSL Library, International Mathematics & Statistical Libraries, INC, Houston Texas 1977.

23 Lazan B.: Damping of Materials and Members in Structural Mechanics, Pergamon Press, Oxford 1968.

24 Leipholtz H.: Stability Theory, Academic Press, New York 1970.

25 Mansour W.M.: Quenching of Limit Cycles of Van der Pol Oscillator, Journal of Sound and Vibration (1972)25(3), 395-405.

26 Matlock H., & Dawkins W.P. and Panak J.J.: A Model for the Prediction of Ice-Structure Interaction, Offshore Technology Conference, Dallas, Texas 1969.

27 Meirovitch L.: Elements of Vibration Analysis, McGraw-Hill, New York 1975.

28 Michel B. and Toussain N.: Mechanisms and Theory of Indentation of Ice Plates, Symposium on Applied Glaciology. Cambridge, September 1976.

29 Minorsky N.: Nonlinear Oscillatiors, D. Van Nonstrand, Toronto 1962.

30 Määttänen M.: Experiences of Ice Forces Against a Steel Lighthouse Mounted on the Seabed, and Proposed Constructional Refinements, POAC-75, University of Alaska, Fairbanks 1975.

31 Määttänen M.: Ice-Force Measurements at the Gulf of Bothnia by the Instrumented Kemi-I Lighthouse, POAC-77, Memorial University of Newfoundland, St John's 1977.

32 Määttänen M.: Stability of Self-Excited Ice-Induced Structural Vibrations, POAC-77, Memorial University of Newfoundland, St John's 1977.

33 Määttänen M.: "Lighthouse or beacon construction", US Patent 3977200, 1976.

34 Neill C.: Force Fluctuations During Ice-Floe Impact on Piers. IAHR Ice Symposium, Leningrad 1972.

35 Neill C.: Dynamic Ice Forces on Piers and Piles. An Assessment of Design Guidelines in the Light of Recent Research, Canadian Journal of Civil Engineering, Vol 3, p 305-341, 1976.

36 Nevel D.E. & Perham R.E. and Hogue G.B.: Ice Forces on Vertical Piles, CRREL Report 77-10, Hanover, April 1977.

37 Pandit S.M. & Subramanian T.L. and Wu S.M.: Stability of Random Vibrations with Special Reference to Machine Tool Chatter, Journal of Engineering for Industry, Trans. ASME, Series B, Vol 97, No 1, pp 216-219, February 1975.

38 Pandit S.M. & Subramanian T.L. and Wu S.M.: Modeling Machine Tool Chatter by Time Series, Journal of Engineering for Industry, Trans. ASME, Series B, Vol 97, No 1, pp 211-215, February, 1975.

39 Parameswaran V.R.: Work Hardening and Strain Rate Sensitivity of Flow Stress in High Purity Ice Single Crystals, CRREL Research Report 342, Hanover, October 1975.

40 Peyton H.R.: Sea Ice Forces, Conference on Ice Pressure against Structures, NRC Technical Memorandum No 92, Laval University, Quebec 1966.

41 Peyton H.R.: Ice and Marine Structures, Ocean Industry, Parts 1, 2 and 3, March, September, December 1968.

42 Reddy, D.V. & Cheema P.S. and Swamidas A.S.J.: Ice Force Response Spectrum Modal Analysis of Offshore Towers, POAC-75, University of Alaska, Fairbanks 1975.

43 Riska K. and Varsta P.: Failure Process of Ice Edge Caused by Impact With Ships Side, Symposium during 100 th Anniversary of Winter Navigation in Finland, University of Oulu, December 1977.

44 Ross B.: Ice Floe-Offshore Platform Interaction, POAC-71, Technical University of Norway, Trondheim 1971.

45 Ross H.E.: Dynamic Response of Offshore Piling, Offshore Technology Conference, Dallas, Texas 1971.

46 Saeki H. & Hamanaka K. and Ozaki A.: Experimental Study on Ice Force on a Pile, POAC-77, Memorial University of Newfoundland, St John's 1977.

47 Schwartz J.: The Pressure of Floating Ice-Fields on Piles, proc. IAHR Symposium on Ice and Its Action on Hydraulic Structures, Reykjavik 1970.

48 Skop R.A. & Ramber S.E. and Ferer K.M.: Added Mass and Damping Forces on Circular Cylinders, Naval Research Laboratory Report 7970, Washington 1976.

49 Swamidas A.S.J. & Reddy D.V. and Purcell G.: Ice-Structure Interaction With Artificially Generated Force Records, Symposium of Applied Glaciology, Cambridge, September 1976.

50 Timoshenko S. & Young D. and Weaver W.: Vibration Problems in Engineering, John Wiley & Sons, New York 1974.

51 Tondl A.: Quenching of Self-Excited Vibrations: Equilibrium Aspects, Journal of Sound and Vibration (1975)42(2), 251-260.

52 Tondl A.: Quenching of Self-Excited Vibrations: Effect of Dry Friction, Journal of Sound and Vibration (1976)42(2), 285-294.

53 Tondl A.: Self-Excited Vibrations, National Research Institute for Machine Design, Monographs and Memoranda No 9, Bechovice 1970.

54 Urabe M.: Nonlinear Autonomous Oscillations, Academic Press, New York 1967

55 Zabilansky L.J. & Nevel D.E. and Haynes F.D.: Ice Forces on Model Structures, Canadian Journal of Civil Engineering, Vol 2 No 4, pp 400-417, 1975

57 Wilkinson J.H.: The Algebraic Eigenvalue Problem, Clarendon Press, Oxford 1965.

58 Wu H.C. & Chang K.J. and Schwartz J.: Fracture in the Compression of Columnar Grained Ice, Engineering Fracture Mechanics, 1976, Vol 8, pp 365-372.

SYMBOLS

A_n	parameter
a	radius of pile
C	parameter
c	shape coefficient
d	diameter of pile
d_{cr}	diameter of ice crystal
F	ice force
F_d	damping force
f	natural frequency
g	gap between ice and structure
H_{ii}	damping coefficient for mode i
h	thickness of ice
k	stiffness coefficient against ice force
L	half diameter of ice floe
t	time
P	force unbalance
X_{ni}	amplitude of mode i at the ice action point n
u_r	radial elastic ice displacement
v_0	constant velocity of ice
v_r	relative velocity between ice and structure
α	parameter
β	parameter
δ	displacement, variation notation
$\dot{\delta}$	velocity
ε_r	radial ice strain
ζ	relative modal damping coefficient
θ	polar angle
κ	coefficient due to aspect ratio d/h

λ	complex root
ξ	perturbation amplitude
ρ	real part of complex root
σ_c	ice crushing strength
$\dot{\sigma}$	stress rate
φ_{nn}	negative ice damping coefficient
Ω	damped natural angular velocity
ω	natural angural velocity
$[A]$	coefficient matrix
$[B]$	coefficient matrix
$[D]$	diagonalized damping matrix
$[d]$	damping matrix
$\{F\}$	force vector
$[I]$	identity matrix
$[K]$	diagonalized stiffness matrix
$[k]$	stiffness matrix
$[M]$	diagonalized mass matrix
$[m]$	mass matrix
$[X]$	eigenvector matrix
$\{x\}$	combined displacement and velocity vector
$\{\dot{x}\}$	combined velocity and acceleration vector
$[0]$	zero matrix
$\{0\}$	zero vector
$\{\delta\}$	displacement vector
$\{\dot{\delta}\}$	velocity vector
$\{\ddot{\delta}\}$	acceleration vector
$\{\xi\}$	perturbation vector
$\{\pi\}$	principal coordinate displacement vector
$\{\dot{\pi}\}$	principal coordinate velocity vector
$\{\ddot{\pi}\}$	principal coordinate acceleration vector
$[\phi]$	negative ice damping matrix

ISBN 951-46-3394-6